



## Quickly erupted volcanic sections of the Steens Basalt, Columbia River Basalt Group: Secular variation, tectonic rotation, and the Steens Mountain reversal

**Nicholas A. Jarboe and Robert S. Coe**

*Department of Earth and Planetary Sciences, University of California, 1156 High Street, Santa Cruz, California 95064, USA (njarboe@pmc.ucsc.edu)*

**Paul R. Renne**

*Berkeley Geochronology Center, 2455 Ridge Road, Berkeley, California 94709, USA*

*Department of Earth and Planetary Science, University of California, Berkeley, California 94720, USA*

**Jonathan M. G. Glen and Edward A. Mankinen**

*U.S. Geological Survey, 345 Middlefield Road, Mail Stop 989, Menlo Park, California 94025, USA*

[1] The Steens Basalt, now considered part of the Columbia River Basalt Group (CRBG), contains the earliest eruptions of this magmatic episode. Lava flows of the Steens Basalt cover about 50,000 km<sup>2</sup> of the Oregon Plateau in sections up to 1000 m thick. The large number of continuously exposed, quickly erupted lava flows (some sections contain over 200 flows) allows for small loops in the magnetic field direction paths to be detected. For volcanic rocks, this detail and fidelity are rarely found outside of the Holocene and yield estimates of eruption durations at our four sections of ~2.5 ka for 260 m at Pueblo Mountains, 0.5 to 1.5 ka for 190 m at Summit Springs, 1–3 ka for 170 m at North Mickey, and ~3 ka for 160 m at Guano Rim. That only one reversal of the geomagnetic field occurred during the eruption of the Steens Basalt (the Steens reversal at approximately 16.6 Ma) is supported by comparing <sup>40</sup>Ar/<sup>39</sup>Ar ages and magnetic polarities to the geomagnetic polarity timescale. At Summit Springs two <sup>40</sup>Ar/<sup>39</sup>Ar ages from normal polarity flows (16.72 ± ± 0.29 Ma (16.61) and 16.92 ± ± 0.52 Ma (16.82); ± ± equals 2σ error) place their eruptions after the Steens reversal, while at Pueblo Mountains an <sup>40</sup>Ar/<sup>39</sup>Ar age of 16.72 ± ± 0.21 Ma (16.61) from a reverse polarity flow places its eruption before the Steens reversal. Paleomagnetic field directions yielded 50 nontransitional directional-group poles which, combined with 26 from Steens Mountain, provide a paleomagnetic pole for the Oregon Plateau of 85.7°N, 318.4°E, K = 15.1, A<sub>95</sub> = 4.3. Comparison of this new pole with a reference pole derived from CRBG flows from eastern Washington and a synthetic reference pole for North America derived from global data implies relative clockwise rotation of the Oregon Plateau of 7.4 ± 5.0° or 14.5 ± 5.4°, respectively, probably due to northward decreasing extension of the basin and range.

**Components:** 12,604 words, 13 figures, 3 tables.

**Keywords:** Steens Basalt; secular variation; Columbia River Basalt; paleomagnetism; magnetostratigraphy; geochronology.

**Index Terms:** 1522 Geomagnetism and Paleomagnetism: Paleomagnetic secular variation; 1525 Geomagnetism and Paleomagnetism: Paleomagnetism applied to tectonics: regional, global; 1115 Geochronology: Radioisotope geochronology.

**Received** 24 April 2008; **Revised** 4 August 2008; **Accepted** 21 August 2008; **Published** 25 November 2008.

Jarboe, N. A., R. S. Coe, P. R. Renne, J. M. G. Glen, and E. A. Mankinen (2008), Quickly erupted volcanic sections of the Steens Basalt, Columbia River Basalt Group: Secular variation, tectonic rotation, and the Steens Mountain reversal, *Geochem. Geophys. Geosyst.*, 9, Q11010, doi:10.1029/2008GC002067.

## 1. Introduction

[2] The Steens Basalt of the Oregon Plateau may cover as much as 50,000 km<sup>2</sup> [Mankinen *et al.*, 1987; Carlson and Hart, 1987] of southeastern Oregon, northwestern Nevada, and northeasternmost California. Its extent, eruptive timing, and relationship to the Columbia River Basalts (CRB) have undergone continued debate. Geochemical and field studies have expanded the traditional Columbia River Basalt Group (CRBG) to include the Steens Basalt [Hooper *et al.*, 2002; Camp *et al.*, 2003; Camp and Ross, 2004; Brueseke *et al.*, 2007] at its base. The relative stratigraphy of the Steens Basalt and the CRBG has been traced over 150 km with relationships determined by an intermediate formation, the basalt of Malheur Gorge [Camp *et al.*, 2003; Brueseke *et al.*, 2007]. The reverse-to-normal (R-N) polarity change as recorded at Steens Mountain (Steens reversal) is believed to be the only reversal to have occurred during the eruption of the Steens Basalt [Mankinen *et al.*, 1987; Camp and Ross, 2004].

[3] We are studying the location, age, and transitional field behavior of the Steens reversal recorded throughout the Oregon Plateau (Figure 1). <sup>40</sup>Ar/<sup>39</sup>Ar age determinations from lavas erupted during the transition [Jarboe *et al.*, 2006; N. Jarboe *et al.*, manuscript in preparation, 2008] place the reversal at 16.69 ± ± 0.14 Ma (16.58). See section 2 for age presentation conventions. Owing to basin and range faulting and little vegetative cover, many thick (>500 m) sections of Steens basalt or their possible equivalents are well exposed and have been studied by others [Watkins, 1963; Brueseke *et al.*, 2007; Mankinen *et al.*, 1987, and references therein]. So far over a dozen locations have been sampled for paleomagnetic and geochronologic study (Figure 1). A forthcoming paper will report on sections studied that record transitional field behavior (N. Jarboe *et al.*, manuscript in preparation, 2008). In this paper we discuss the paleomagnetic and geochronologic results from four sections that record stable polarity secular variation: Summit Springs (60 km northeast of Steens Mountain), Pueblo Mountains (65 km south of Steens Mountain), North Mickey (25 km east of Steens Moun-

tain), and Guano Rim (95 km southwest of Steens Mountain). Except for one lava at Summit Springs, each section erupted during a single geomagnetic polarity chron, and <sup>40</sup>Ar/<sup>39</sup>Ar data, stratigraphy, and petrological considerations place their eruptions in chrons just before or after the Steens reversal. Although some others believe that the Steens Basalt gradually erupted over millions of years [Brueseke *et al.*, 2007], we will show that magnetic field behavior, field polarity, and geochronology of these sections are consistent with rapid local emplacement (1–3 ka) within ~300 ka of the Steens reversal.

## 2. Age Data Presentation

[4] Ages in early literature were usually reported with one sigma uncertainty, while two sigma is commonly reported today. We suggest (and herein adopt) using ± to represent exclusively one sigma, ± ± to indicate two sigma, and ±<sup>x</sup> to indicate an x% confidence interval. For example ±<sup>95</sup> would represent an uncertainty at the 95% confidence interval. This convention is used for ages throughout this paper, with standard paleomagnetic conventions used elsewhere. When citing values with uncertainties from other work, we prefer to present the uncertainty given in the original and convert to other uncertainties if needed for clarity.

[5] We present ages here using the Fish Canyon sanidine (FCs) age of 28.201 ± ± 0.214 Ma determined by astronomical calibration [Kuiper *et al.*, 2008] and the <sup>40</sup>K decay constant of 5.463 ± ± 0.107 × 10<sup>-10</sup>/a [Steiger and Jager [1977], updated by Min *et al.* [2000]]. To ease comparison to other <sup>40</sup>Ar/<sup>39</sup>Ar ages in the literature, the <sup>40</sup>Ar/<sup>39</sup>Ar ages determined using the Earthtime (An NSF supported international scientific initiative; <http://www.earth-time.org>) conventions of 28.02 Ma for the FCs [Renne *et al.*, 1998] and 5.543 ±<sup>95</sup> 0.089 × 10<sup>-10</sup>/a for the <sup>40</sup>K decay constant [Steiger and Jager, 1977] are included in parenthesis after each age.

## 3. Paleomagnetic Procedures

[6] All paleomagnetic procedures and analyses were performed at the University of California,

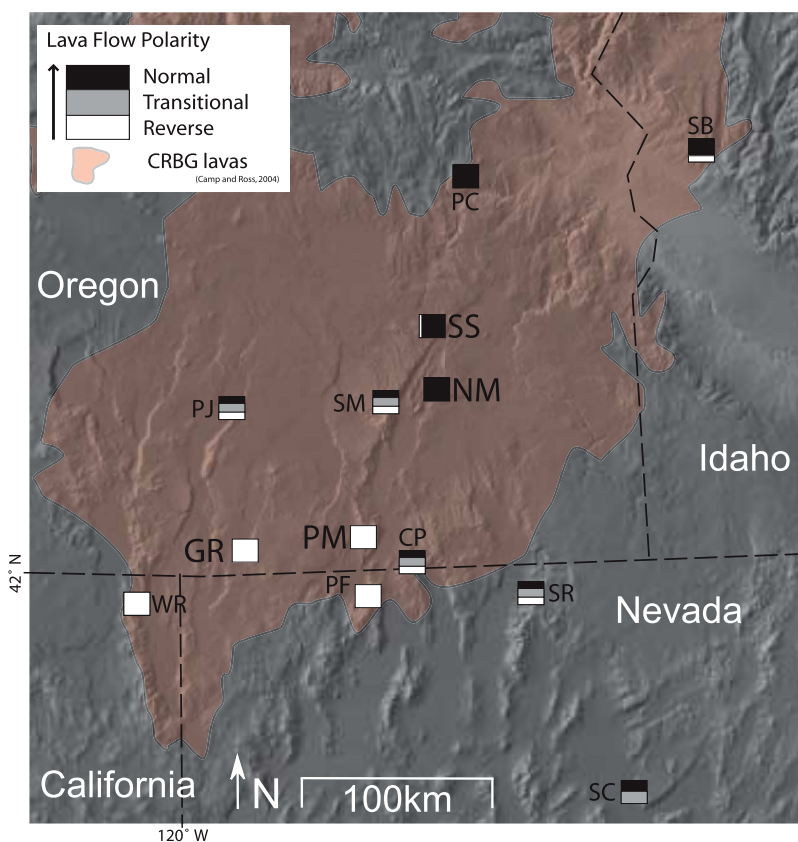


**Figure 1.** Location and magnetic polarity of volcanic sections. CP, Catlow Peak, GR, Guano Rim, NM, North Mickey, PC, Pole Creek, PF, Pine Forest, PJ, Poker Jim Ridge, PM, Pueblo Mountains, SB, Squaw Butte (Imnaha), SC, Sheep Creek, SM, Steens Mountain, SR, Santa Rosa, SS, Summit Springs (where the stratigraphic relationship of a single reversed polarity flow with respect to the main normal polarity section is uncertain), WR, Warner Range.

Santa Cruz unless otherwise noted. Paleomagnetic cores were sampled with a 2.5 cm diameter, water-cooled, diamond-studded, hollow core bit using a handheld gasoline powered drill. The cores were drilled 5–10 cm deep, oriented to an accuracy of  $1^{\circ}$ – $2^{\circ}$  while still attached to the outcrop using an orienting stage and a Brunton compass. Sun sites, sun shadows, and site points of known direction were used to correct for local magnetic anomalies.

Flow bottoms were generally drilled to minimize the chance of remagnetization by overlying flows. The orientation angles were recorded to the nearest degree and time to the nearest minute. Cores were later cut into 2.5 cm long specimens back at the laboratory. In general the deepest, least weathered specimens from each core were used when determining the paleomagnetic field directions.

**Figure 2.** (a) Well behaved alternating field (AF) demagnetization to 190 mT of normally magnetized specimen nm0305a from the North Mickey section. Natural remanent magnetization (NRM) is 3.9 A/m. (b) Orthogonal vector diagram in stratigraphic coordinates of specimen pm12A02a from the Pueblo Mountains section which dips  $20^{\circ}$  to the west. The normal viscous overprint is removed at about 11 mT and then the reversed characteristic remanent magnetization (ChRM) decays univectorially toward the origin. The overprint direction is to the west of the expected geocentric axial dipole (GAD) field but is very close to the expected GAD field in geographic coordinates, indicating that it is a normal viscous overprint acquired after tilting of the section during the most recent (Brunhes) normal polarity chron. NRM = 2.6 A/m. (c) Orthogonal vector diagram showing complete removal from specimen pm0402a of a westerly lightning isothermal remanent magnetism (IRM) by 25 mT AF demagnetization. The ChRM then decays univectorially toward the origin between 25 and 180 mT. NRM = 4.7 A/m. (d) Stereonet plot of the AF demagnetization of the same specimen (pm0402a); lightning IRM is removed by 25 mT. (e) Stereonet plot of the AF demagnetization to 180 mT of specimen pm0407a from the same flow as Figures 2c and 2d shows a strong lightning overprint which is not completely removed but the great circle path is heading toward the flow mean direction. NRM = 17.3 A/m.

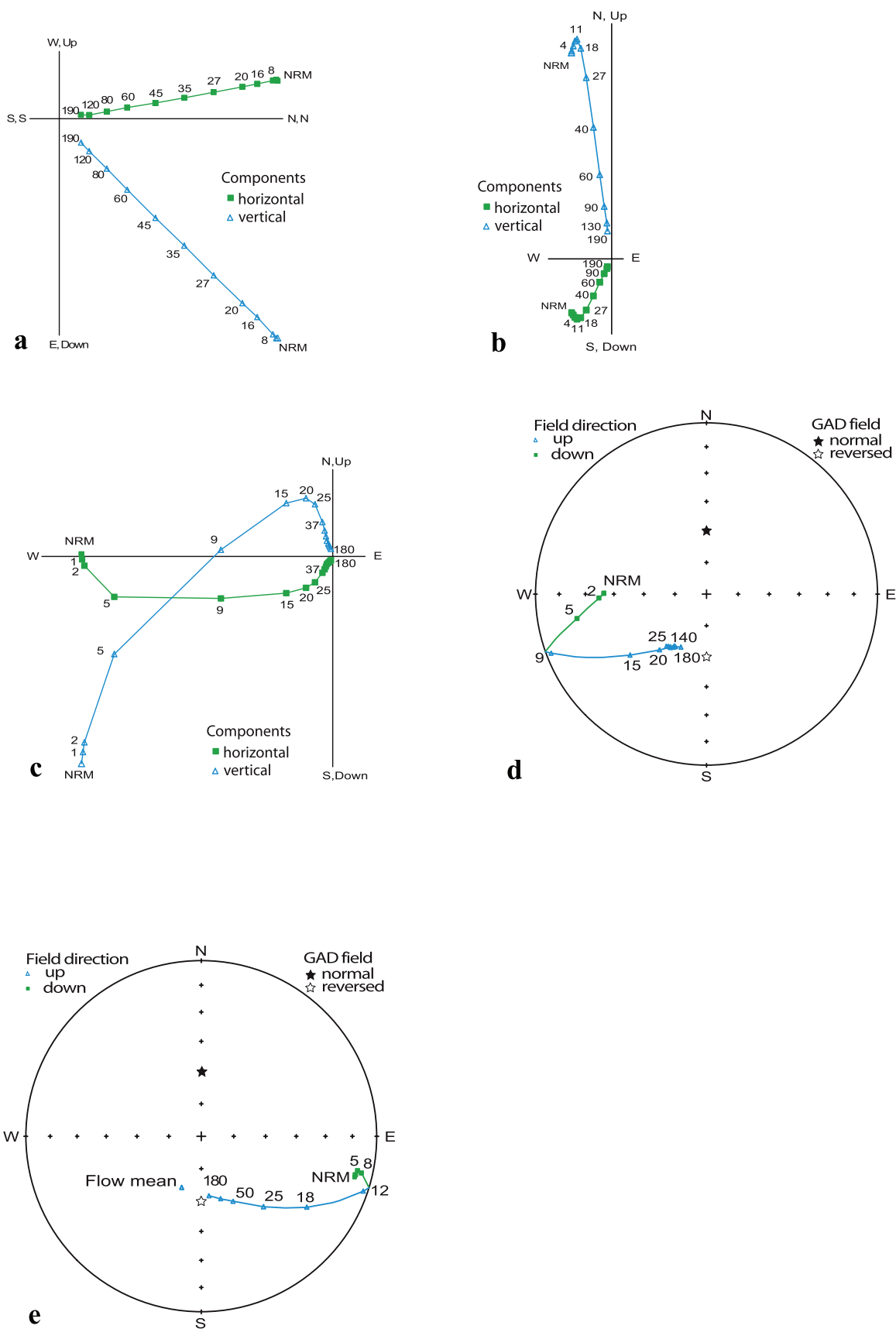
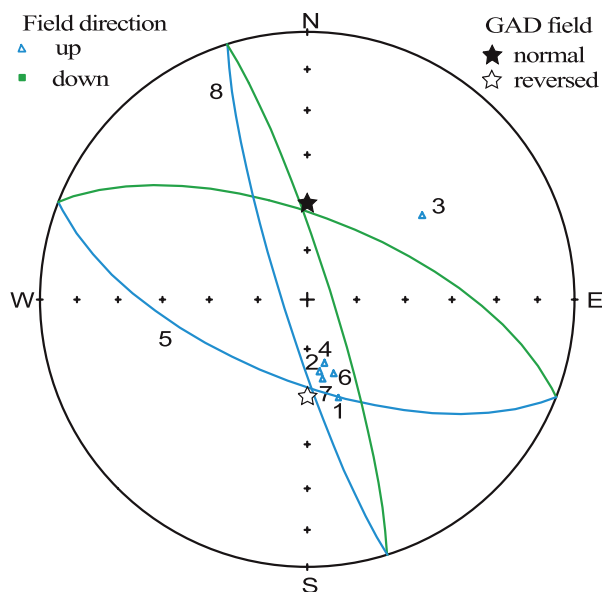


Figure 2



**Figure 3.** Determining the flow mean direction of flow 9 at the Pueblo Mountains section. Specimens 1, 2, 4, 6, and 7 yielded stable directions that decayed univectorially to the origin. Specimens 5 and 8 were overprinted with lightning but decayed along great circles toward the cluster of stable directions. Specimen 3 was rejected from the mean as an outlier. Its anomalous direction may be due to orientation error, core labeling error, or taken from a block that had moved. These outliers are rare. This flow mean direction was determined by the method of *McFadden and McElhinny* [1995].

[7] The natural remanent magnetization (NRM) of the specimens was stepwise-demagnetized in a decaying alternating field (AF) of up to 200 mT and magnetizations were measured in a 2G superconducting magnetometer. Twelve-position measurements were made using custom built hardware and software. An Agico JR-5 calibration sample was measured at least daily and kept within  $1.2^\circ$  of the expected direction with an estimated error no greater than  $1.2^\circ$ . The characteristic remanent magnetization (ChRM) direction of each specimen was determined with straight line to the origin fits [*Kirschvink*, 1980] and occasional great circles [*McFadden and McElhinny*, 1988] using PMGSC42 software [*Enkin*, 2005]. Most specimens were well-behaved upon stepwise AF-demagnetization (Figure 2a). Any viscous component was typically removed by 2 to 15 mT (Figure 2b). A few specimens taken from near lightning strikes required greater demagnetization fields to reveal the ChRM, but in most cases a well defined direction was determined (Figures 2c and 2d). In areas of unusually strong lightning remagnetization, some

specimens were overprinted with magnetizations that were not removed even at the highest ( $\sim 200$  mT) demagnetization steps (Figure 2e). In such cases the magnetic direction during AF demagnetization usually followed a great circle toward the ChRM direction (Figure 2e).

[8] Generally, at least eight samples were taken from each flow and the mean flow directions were determined using *Fisher* [1953] or *McFadden and McElhinny* [1995] statistics (Figure 3). Directions, virtual geomagnetic poles (VGPs), and other data for the flows are shown in Table 1. Three flows at Summit Springs yielded too few ChRMs or great circle fits to determine mean flow directions. In the remaining flows 658 cores were measured, and of these 570 had resolvable characteristic directions, 72 yielded acceptable great circle fits, and 16 directions were rejected. Of the rejected directions, eight had lightning overprints so strong as to completely overwhelm the ChRM, one had an unstable demagnetization path, and seven had resolvable characteristic directions but with outlying directions far ( $>40^\circ$ ) from the flow mean direction. These rare outlying directions are likely due to misorientation of the core, undetected post-eruptive movement of the sampled outcrop, or complete overprinting.

#### 4. Sampling Strategy and Grouping Flow Directions

[9] The volcanic sections presented here were sampled as part of our search for lava flows erupted during the Steens reversal to shed light on transitional field behavior. For this reason we chose flow-on-flow sections, where exposure is high, stratigraphy is straightforward, and cover between flows that might conceal a long eruption hiatus or other geological complexity is minimal (see Figures S1 and S2 in the auxiliary material for photos).<sup>1</sup> If measurements in the field with a handheld-fluxgate magnetometer suggested lava flows with intermediate polarity, then we sampled almost every flow unit. If not, we still sampled the section in case overprints obscured a transition zone, usually skipping some lava flows that could be acquired on a return visit if a transition were found, so that we could cover a greater interval. For studies of secular variation in flow-on-flow sections such as these, skipping some flows is common practice because the episodic nature of

<sup>1</sup>Auxiliary materials are available in the HTML. doi:10.1029/2008GC002067.

**Table 1.** Paleomagnetic Field Directions, VGPs, and Geographic Locations of the Flows and the Directional Groups From the Summit Spring, Pueblo Mountains, North Mickey, and Guano Rim Sections<sup>a</sup>

DG	Flow ID	N <sub>0</sub>	N	LF	GC	D°	I°	k	α <sub>95</sub>	Long°	Lat°	A <sub>95</sub>	FNS	°N	°W	el(m)
<i>Summit Springs</i>																
1	ss16	8	7	6	1	32.5	40.0	242	3.9	358.4	56.3	3.6	2	43.10826	118.25877	1658
2	ss14	8	8	6	2	25.3	40.2	77.1	6.5	7.6	60.9	6.1	2	43.10841	118.25872	1658
3	ss13	8	7	3	4	333.7	30.9	170	5.0	110.1	55.4	4.2	3–6	43.10846	118.25919	1660
4	ss12	8	6	0	6	339.4	36.6	1130	2.6	105.4	61.5	2.3	2	43.10839	118.25942	1684
5	ss09	8	6	5	1	50.1	65.6	321	3.8	306.2	55.2	5.6	3	43.10919	118.26141	1709
5	ss08	8	8	4	4	46.3	65.1	174	4.4	308.2	57.6	6.4	2	43.10934	118.26199	1739
6	ss07	8	8	4	4	16.3	79.7	65.9	7.2	253.4	61.8	13.5	4–5	43.11051	118.26507	1759
7	ss06	8	8	6	2	10.3	63.6	214	3.9	312.2	82.3	5.5	3–4	43.11119	118.26589	1779
8	ss05	8	8	6	2	26.4	57.4	347	3.3	337.0	69.4	4.1	2	43.11109	118.26679	1780
8	ss04	8	8	4	4	20.3	67.2	76.5	6.7	298.4	74.5	10.2	2–3	43.11152	118.26826	1819
8	ss03	8	7	4	3	31.2	60.0	57.8	8.4	326.4	66.8	11.1	0	43.11164	118.26866	1814
9	ss02	8	8	6	2	53.7	67.2	438	2.7	301.8	53.2	4.1	0	43.11234	118.26997	1846
10	ss01	8	8	8	0	57.7	61.7	346	3.0	311.4	48.7	4.1	n/a	43.11242	118.27026	1843
11	ss18 <sup>b</sup>	8	8	8	0	225.4	–74.2	334	3.0	103.0	–57.9	5.2	n/a	43.11088	118.24488	1540
<i>Grouped Flows</i>																
5	ss8–9	15	14	9	5	48.1	65.4	240	2.6	307.1	56.4	3.8				
8	ss3–5	24	23	14	9	26.5	62.0	72.8	3.6	322.1	70.8	4.9				
<i>Devine Canyon Tuff<sup>c</sup></i>																
	ss17	9	7	3	4	4.9	54.4	147	5.5					43.01108	118.25083	1552
<i>Pueblo Mountains</i>																
1	pm08	8	7	7	0	190.8	–57	32	10.8	177.4	–80.5	13.4	1	42.05015	118.68622	2072
2	pm07	8	7	7	0	158.1	–70	397	3.0	16.5	–71.6	4.8	4	42.05112	118.68600	2105
3	pm06	8	7	5	2	179.7	–56	314	3.5	243.8	–84.5	4.3	0	42.05190	118.68682	2143
4	pm05	8	8	2	6	201.5	–55	155	4.9	165.1	–72.2	5.9	2	42.05160	118.68785	2152
5	pm04	8	8	2	6	196.4	–64	110	5.8	129.3	–77.7	8.2	0	42.05353	118.68923	2158
5	pm03	8	7	7	0	191.7	–62	148	5.0	143.8	–81.3	6.8	1	42.06265	118.69517	2213
5	pm02	7	7	7	0	193.3	–57	251	3.8	168.8	–79.0	4.8	2	42.06270	118.69718	2258
5	pm01	8	8	7	1	188.5	–62	395	2.8	134.9	–83.6	3.9	0	42.06263	118.69827	2311
6	pm12A	8	8	8	0	198.4	–69	368	2.9	103.7	–73.6	4.6	0	42.06261	118.69840	2327
7	pm13	8	8	8	0	214.5	–70	844	1.9	112.8	–64.5	3.0	0	42.06298	118.69896	2333
8	pm14	8	6	3	3	166.4	–65	233	4.7	1.5	–79.3	6.8	n/a	42.06293	118.69942	2336
9	pm10 <sup>(a)</sup>	8	8	8	0	185.9	–42	431	2.7	224.0	–71.7	2.6	n/a	41.96818	118.71892	n/a
10	pm11 <sup>(a)</sup>	8	7	3	4	214.9	–35	313	3.7	178.3	–52.7	3.2	n/a	41.96960	118.72093	1729
11	pm09 <sup>(a)</sup>	8	7	5	2	168.2	–65	249	3.9	4.2	–80.4	5.6	n/a	41.91142	118.73543	1343
10	pm12 <sup>(a)</sup>	7	7	2	5	217.7	–36	93.0	6.9	174.6	–51.2	6.1	n/a	41.91172	118.73623	1377
<i>Grouped Flows</i>																
5	pm1–4	31	30	23	7	191.7	–61.3	176	2.0	145.4	–81.3	2.7				
10	pm11–12	15	14	5	9	216.0	–35.6	162	3.2	176.5	–52.3	2.8				
<i>North Mickey</i>																
1	nm01	8	7	7	0	13.8	61.6	127	5.4	327.2	79.9	7.3	0	42.76763	118.29797	1309
2	nm02	8	8	7	1	19.3	58.2	190	4.1	340.2	74.9	5.2	0			
3	nm03	8	8	8	0	349.4	45.7	204	3.9	93.9	72.1	4.0	0	42.76781	118.29733	1318
3	nm04	8	8	8	0	348.7	45.2	659	2.2	95.1	71.5	2.2	0	42.76789	118.29731	1318
4	nm05	8	8	7	1	346.9	53.2	387	2.8	114.6	76.3	3.2	0	42.76796	118.29732	1326
5	nm06	8	8	7	1	325.4	56.1	365	2.9	150.4	62.9	3.5	0	42.76797	118.29619	1337
6	nm07	8	8	8	0	331.4	52.8	75.5	6.4	138.4	65.7	7.4	0			
7	nm08	8	8	8	0	36.8	65.2	161	4.4	309.1	63.9	6.4	0			
7	nm09	8	8	8	0	37.3	63.0	496	2.5	315.2	63.2	3.5	0			
7	nm10	8	8	8	0	39.0	64.2	232	3.6	311.6	62.2	5.1	0			
7	nm11	8	8	7	1	28.5	64.1	407	2.8	313.3	69.5	4.0	0			
8	nm12	8	8	7	1	18.8	53.6	407	2.8	356.0	73.0	3.3	0	42.76870	118.29663	1398
9	nm13	8	8	8	0	4.1	63.9	226	3.7	286.8	86.0	5.3	0	42.76885	118.29650	1411
10	nm14	8	8	8	0	347.8	60.4	274	3.4	146.8	80.8	4.5	0			
11	nm15	8	8	8	0	346.8	58.9	137	4.7	138.6	79.6	6.1	0	42.76894	118.29632	1444
11	nm16	8	8	8	0	356.0	49.2	311	3.1	77.1	76.9	3.3	1			

**Table 1.** (continued)

DG	Flow ID	N <sub>0</sub>	N	LF	GC	D°	I°	k	α <sub>95</sub>	Long°	Lat°	A <sub>95</sub>	FNS	°N	°W	el(m)
12	nm17	8	8	8	0	336.4	43.7	243	3.6	117.5	64.1	3.5	4	42.76939	118.29607	1481
13	nm22	8	8	8	0	10.7	62.9	435	2.7	316.8	82.1	3.8	3	42.76970	118.29568	1463
14	nm26	8	8	6	2	25.3	56.7	212	3.9	339.1	69.9	4.8	5	42.77025	118.29620	1526
15	nm32	8	8	8	0	8.1	59.0	105	5.4	355.5	83.2	7.0	2	42.77091	118.29639	1574
16	nm35	8	8	7	1	337.1	49.4	124	5.2	124.7	67.8	5.6	n/a	42.77169	118.29689	1628
<i>Grouped Flows</i>																
3	nm3–4	16	16	16	0	349.1	45.5	331	2.0	94.5	71.9	2.0				
7	nm8–11	32	32	31	1	35.6	64.2	253	1.6	312.2	64.6	2.3				
11	nm15–16	16	16	16	0	352.0	54.2	101	3.7	102.0	79.8	4.4				
<i>Guano Rim</i>																
1	gr02	8	8			189.9	–50.5	987	1.8	201.2	–76.6	2.0	0			
1	gr03	7	7			189.1	–53.1	206	4.2	197.2	–78.9	4.8	0			
1	gr04	8	8			190.8	–48.9	782	2.0	201.7	–75.0	2.1	0			
2	gr05	8	8			193.2	–51.4	874	1.9	190.0	–75.5	2.1	0			
2	gr06	7	7			196.8	–47.1	478	2.8	190.5	–70.6	2.9	0			
2	gr07	9	9			194.3	–45.9	324	2.9	197.7	–71.1	3.0	0			
2	gr08	9	9			192.6	–51.1	781	1.8	192.2	–75.6	2.0	2			
2	gr11	8	8			194.5	–47.3	1486	1.4	195.1	–72.0	1.5	0			
2	gr12	9	9			191.9	–48.9	1900	1.2	198.7	–74.4	1.3	0			
2	gr13	7	7			198.9	–48.2	312	3.4	184.6	–70.0	3.6	0			
3	gr14	9	9			223.7	–63.4	202	3.6	130.2	–58.6	5.1	0			
4	gr15	8	8			191.7	–68.9	120	5.1	94.1	–77.1	8.0	0			
4	gr16	8	8			189.0	–68.6	652	2.2	89.3	–78.4	3.4	0			
4	gr17	8	8			183.1	–66.2	117	5.2	78.0	–83.2	7.7	2			
5	gr20	8	8			198.8	–66.8	233	3.6	114.9	–75.0	5.4	1			
6	gr22	8	8			209.2	–65.1	255	3.5	126.8	–68.7	5.1	1			
7	gr24	6	6			197.3	–21.8	583	2.8	209.3	–55.7	2.1	0			
7	gr25	6	6			199.6	–23.4	748	2.5	205.0	–55.6	1.9	2			
7	gr28	6	6			196.3	–16.0	103	6.6	212.9	–53.1	4.9	0			
7	gr29	8	8			197.6	–18.2	693	2.1	210.2	–53.8	1.6	0			
7	gr30	8	8			196.1	–15.1	228	3.7	213.5	–52.8	2.7	0			
7	gr31	6	6			199.0	–17.3	516	3.0	208.4	–52.8	2.2	3			
7	gr35	8	8			196.4	–19.5	1661	1.4	211.6	–54.9	1.1	0			
8	gr36	8	8			193.9	–56.2	264	3.4	172.4	–78.0	4.2	0			
9	gr37	8	8			193.5	–61.2	322	3.1	144.9	–80.0	4.2	3			
9	gr41	8	8			190.1	–61.0	1093	1.7	147.5	–82.5	2.3	0			
9	gr42	8	8			194.2	–61.3	659	2.2	144.1	–79.5	3.0	1			
10	gr44	9	9			193.8	–65.9	1158	1.5	113.7	–78.5	2.2	0			
11	gr45	8	8			198.3	–69.2	677	2.1	103.2	–73.7	3.3	0			
12	gr46	9	9			193.7	–63.9	868	1.7	126.4	–79.5	2.4	0			
12	gr47	8	8			198.5	–65.1	1056	1.7	123.2	–75.9	2.5	0			
12	gr48	9	9			195.0	–65.1	944	1.7	120.1	–78.2	2.5	0			
12	gr49	8	8			192.3	–62.1	812	1.9	138.4	–80.9	2.6	n/a			
<i>Grouped Flows</i>																
1	gr02–04	23	23			190.0	–50.7	394	1.5	200.5	–76.7	1.7				
2	gr05–13	57	57			194.5	–48.6	414	0.9	192.9	–72.9	1.0				
4	gr15–17	24	24			187.8	–67.9	163	2.3	89.1	–79.7	3.5				
7	gr24–35	48	48			197.1	–18.6	289	1.2	210.8	–54.2	0.9				
9	gr37–42	24	24			192.6	–61.2	553	1.3	144.7	–80.6	1.7				
12	gr46–49	34	34			194.8	–64.1	729	0.9	125.8	–78.7	1.3				

<sup>a</sup>Flows are listed from oldest to youngest reading downward in the table unless otherwise noted. Flow mean directions were calculated using PMGSC4.2 software by Randy Enkin. Sections are flat-lying except for Pueblo Mountains where the data was corrected for a tilt striking 180° dipping 20° W. DG is the identification number for each group of directions, Flow ID is the label given the flow in the field, N<sub>0</sub> is the number of cores taken from the flow, N is the number of specimens used to determine mean flow direction, LF (GC) is the number of specimens with magnetic directions determined by a line-fit to the origin (great circle fits), D (I) is the mean magnetic declination (inclination) of the flow, k is the precision parameter of the mean direction, α<sub>95</sub> is the 95% confidence limit on the mean direction, Long (Lat) is the longitude (latitude) of the virtual geomagnetic pole (VGP), A<sub>95</sub> is the 95% confidence limit on the VGP, FNS is the number of flows not sampled between the flow and the next higher one, el is the elevation of the flow from handheld GPS, n/a is not available or not applicable.

<sup>b</sup>Flow not in stratigraphic order.

<sup>c</sup>Much younger ash flow tuff found at the bottom of the Summit Springs section. Directional data presented for completeness.

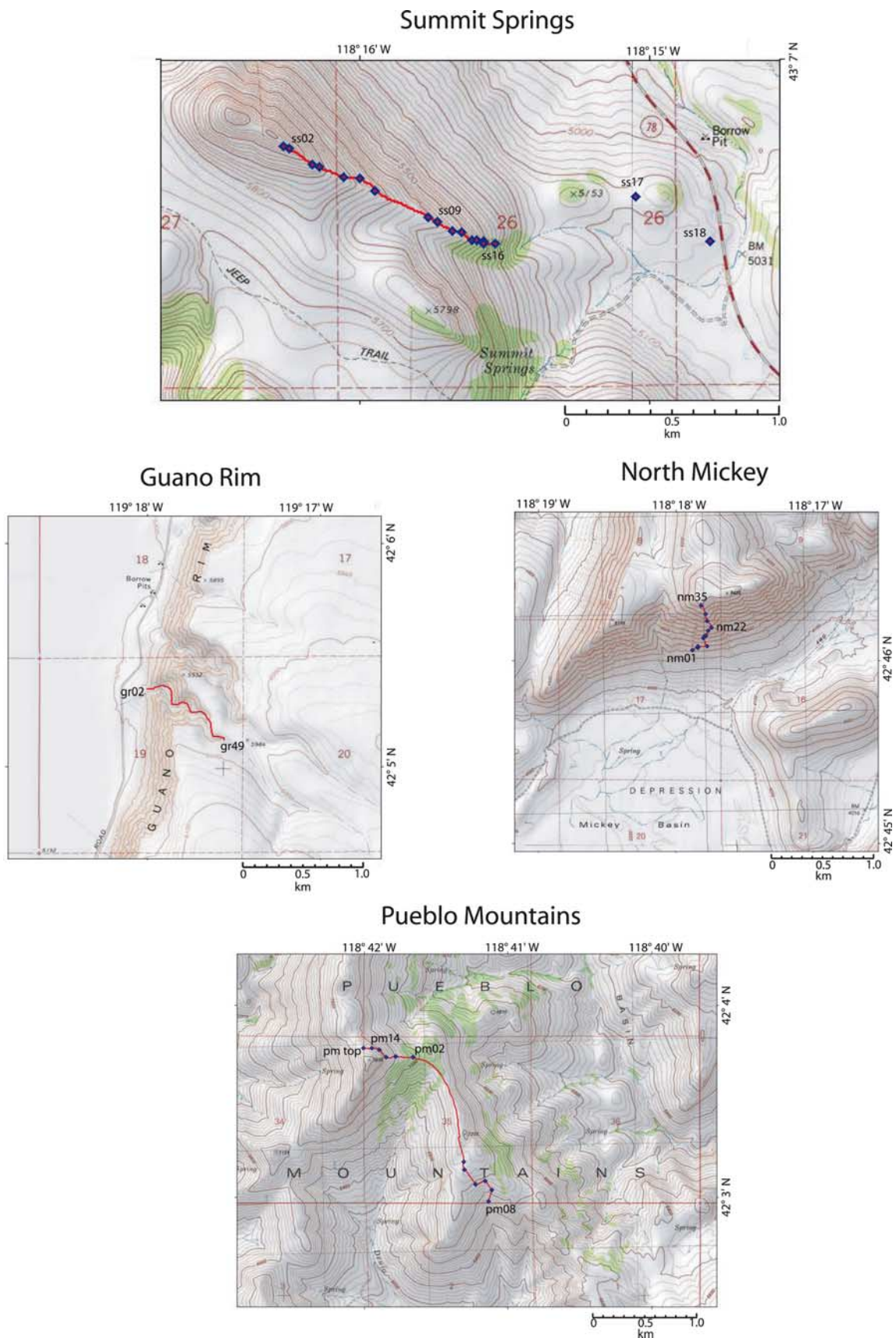


**Figure 4.** Shaded contour maps of the four sections. Selected sample locations marked.

volcanism results in packets of successive lavas that span little time and have directions that are the same or very similar. To test that this is the cause rather than extended intervals of unchanging field direction, geochemical analyses of some of these packets are being performed under the assumption that little magma differentiation occurs during a burst of frequent eruptions.

[10] Nonetheless, we still encountered some repetitions of the same or very similar directions in stratigraphically ordered flows. Following the practice of earlier studies at Steens Mountain, these flow packet directions are combined into directional groups (DGs) by the method described by *Mankinen et al.* [1985]. Specifically, lava flow mean directions that are in sequence and whose  $\alpha_{95}$  values overlap are combined unless they trend in a consistent direction, in which case the flows are not grouped. After this procedure there are 50 remaining directions, of which 13 represent averages of more than one flow and 37 that are individual flow directions. All the directions for individual lava flows, as well as the grouped-flow directions, are given in Table 1. The mean direction for each of the four sections do not differ significantly whether computed from the directional groups or from the individual flows, but the confidence circles are a little larger when flows are grouped because  $N$  is smaller. In general, we expect that the grouped data provide a more representative sampling of secular variation, and thus the directions and VGPs shown in the figures are for the DGs unless otherwise noted.

## 5. $^{40}\text{Ar}/^{39}\text{Ar}$ Geochronology Procedures

[11] All sample preparation and analyses for  $^{40}\text{Ar}/^{39}\text{Ar}$  geochronology were done at the Berkeley Geochronology Center (BGC). Plagioclase, sanidine, or groundmass aliquots were prepared from either alteration-trimmed rocks from the same flows as the paleomagnetic cores or the paleomagnetic cores themselves. These samples were crushed, washed, and sieved into size fractions. Each size fraction used was magnetically separated with a Frantz Isodynamic Separator, washed ultrasonically in a dilute (3–4%) HF solution for 3–5 min, and rinsed in a purified water sonic bath for 20–40 min. The samples were then hand-picked under a microscope. For plagioclase and sanidine aliquots, clear grains were selected and any grains with visible inclusions or surface alteration were discarded. Individual groundmass grains were selected to exclude any containing phenocryst frag-

ments. These aliquots and Fish Canyon sanidine (FCs) grains were then placed into separate pits in aluminum disks, wrapped tightly in aluminum foil, and irradiated for 5 h in the CLICIT facility of the TRIGA reactor at Oregon State University. The neutron fluence ( $J$  parameter) experienced by each aliquot was calculated using an age of 28.02 Ma [*Renne et al.*, 1998] from the FCs standards which had been placed in the center and around the edge of the disk. After waiting typically 4–6 months for  $^{37}\text{Ar}$  to decay to optimal measurement levels, samples were degassed with a  $\text{CO}_2$  laser and the argon isotopes were analyzed with an online MAP 215C mass spectrometer. Samples were then heated in steps for plagioclase and groundmass samples and to total fusion or in steps for single grains of sanidine. Analysis of the empty chamber and atmospheric argon were run often to determine the blank correction and the spectrometer's mass discrimination, respectively. Parabolic or linear curves were fit to the individual ion beam intensity versus time data to determine the relative abundances of the  $^{40}\text{Ar}$ ,  $^{39}\text{Ar}$ ,  $^{38}\text{Ar}$ ,  $^{37}\text{Ar}$ , and  $^{36}\text{Ar}$  isotopes found in the sample. The plateau ages were then determined with the program Mass Spec version 7.621 [*Deino*, 2001] using 95% indistinguishability confidence criterion applied to at least 50% of the  $^{39}\text{Ar}$  released comprising at least three contiguous steps unless otherwise stated. Weighted (by inverse variance) mean ages from multiple single-grain plateau ages were determined with Isoplot 3.66 [*Ludwig*, 2003].

## 6. Volcanic Sections: Geology and Paleomagnetism

### 6.1. Pueblo Mountains

[12] The reverse polarity Steens-like Pueblo Mountains section (42.1°N, 118.7°W) is 60 km south of Steens Mountain at the southern end of the Steens Mountain escarpment (Figure 4; photos and larger-scale map in Figure S1). The Steens Basalts were first described at the type section at Steens Mountain by *Fuller* [1931, p. 102]: “The rock is distinctive in the field both from a peculiar porous texture, which is quite characteristic, and from its local content both of labradorite phenocrysts ranging from 1 to 4 cm. in length, and of olivine grains, which are predominantly under 2 mm. in diameter.” (See photos in Figure S3.) Unlike the Steens-type section, which is underlain by mid-Miocene volcanics, the Pueblo Mountains section is unconformably underlain by crystalline Middle Creta-

ceous intrusive and metamorphic basement [Hart *et al.*, 1989]. We sampled 11 of about 20 flow-on-flow lavas from a continuous section extending across 2.3 km and spanning 260 m of elevation. Four other flows located to the south of the main section were also sampled in an unsuccessful attempt to find normal polarity lava flows from the overlying normal polarity chron. Flows in the Pueblo Mountains are tilted 20°W about a strike of 180° and our paleomagnetic field directions have been corrected accordingly. The attitude of the beds was determined by field measurements and is in good agreement with 1:24,000 scale mapping of the area by Rowe [1971].

[13] The mean direction for each flow at Pueblo Mountains is given in Table 1. To estimate how long the changes in magnetic directions took, we compare the record of the continuous section to a high-resolution historical record from Germany [Schnepf and Lanos, 2005]. Their record encompasses the last 2600 years from sites with similar latitudes and geographical extent as our study area (Figure 5a). The directions span about 30° east-to-west and 15° north-to-south with the whole area traversed in about 2000 years. Smaller loops of the field are also made during the main traverse. The lower-resolution record at Pueblo Mountains is comparable (Figure 5b). It makes a little over one large loop with some internal complexity that is suggestive of a small loop. The secular variation behavior of the field is similar to that observed in other high-resolution records [Ohno and Hamano, 1992; Hagstrum and Champion, 2002]. Assuming that the geomagnetic field at 16.6 Ma behaved similarly to the modern field, the record suggests that the Pueblo Mountains section erupted in about 2500 years. Also supporting a short eruption duration is the low dispersion of VGPs (14.6°), which is significantly less than the 21.2° estimated for full secular variation during this period of geologic time [McFadden *et al.*, 1991]. Thus we conclude that the upper ~250 m of the section of Steens-like lavas at Pueblo Mountains erupted in about 2.5 ka.

## 6.2. Summit Springs

[14] The section at Summit Springs (43.1°N, 118.3°W) is 60 km northeast of Steens Mountain at the northern end of the Steens Mountain escarpment (Figure 4, photos in Figure S2). It consists of approximately 50 normally magnetized flow-on-flow lavas in a well-exposed 190 m thick section. Many of these Steens Basalts are plagioclase-rich with plate-like crystals up to 3 cm in length. The

section is covered at the bottom by the much younger Devine Canyon Tuff, which flowed south out of the Harney Basin over some existing topography (V. Camp, personal communication, 2005). Under the tuff, 1 km east of the bottom of the section, a reverse polarity flow is exposed in a road cut adjacent to State Highway 78. This basalt is not Steens-like in appearance and does not contain the large plagioclase crystals found in many Steens basalt flows, setting it apart from the other flows at Summit Springs. Given its uncertain stratigraphic relationship with the main section and its problematic <sup>40</sup>Ar/<sup>39</sup>Ar age determination, this flow could have erupted before or after the Steens reversal. Even with this stratigraphic uncertainty, we include its magnetic direction in the mean pole calculation as it almost certainly erupted within 1 Ma of the Steens reversal.

[15] Eighteen horizontal flows were sampled, 15 of which gave directions consistent enough to calculate flow mean directions (Table 1). Flow ss17 is the younger Divine Canyon Tuff and is not discussed further. Comparison of the Summit Springs directional path to that of Steens Mountain is done without correcting for latitude because the geocentric axial dipole (GAD) field inclination differs by less than half a degree between the two sites. This is much less than other errors such as those related to bedding corrections or core orientation.

[16] The beginning and end of the directional path as recorded at Summit Springs (Figures 6a and 6b) has some similarities to the path at the end of the reversal at Steens Mountain (Figures 6c and 6d) [Mankinen *et al.*, 1985], but the sense of movement in the middle of the two records is different. The first five field directions (DGs 1–5) from the bottom of the section at Summit Springs span a large angle representing an unknown amount of time. In the upper part of the section (DGs 5–10) a small loop of the field suggests an eruption duration of about 500–1500 years when compared to Holocene records. In conclusion, based on <sup>40</sup>Ar/<sup>39</sup>Ar ages and paleomagnetic arguments, the upper 150 m of lavas at Summit Springs is likely to have erupted over 500–1500 years, possibly immediately after the Steens reversal.

## 6.3. North Mickey

[17] The section at North Mickey (42.8°N, 118.3°W) is 25 km east of Steens Mountain at the north end of the Mickey Basin (Figure 4). The section is on a down-dropped block of Steens Basalt as mapped by Hook [1981] and “correlation

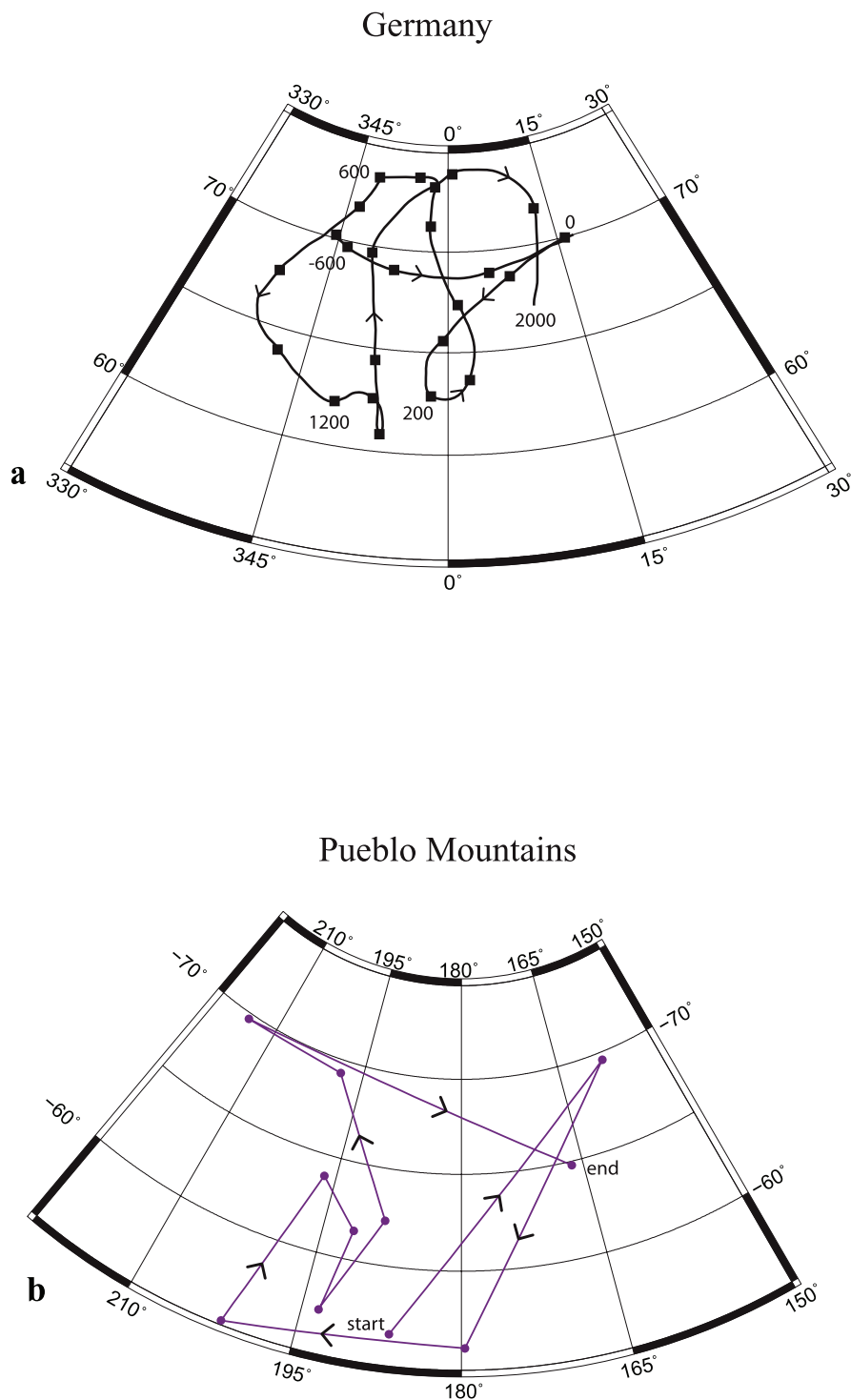


**Figure 5.** (a) Secular variation from a similar latitude as the study area. The historical magnetic field direction as determined from archeological artifacts in Germany, 600 BC to present (data from *Schnepf and Lanos* [2005]). (b) At Pueblo Mountains the field movement makes a little over one loop with some internal complexity. Comparison to a modern magnetic field movement record at a similar latitude (see above) suggests an eruption duration of 1–2 ka. All flows (not directional groups) are shown, from the continuous section only.

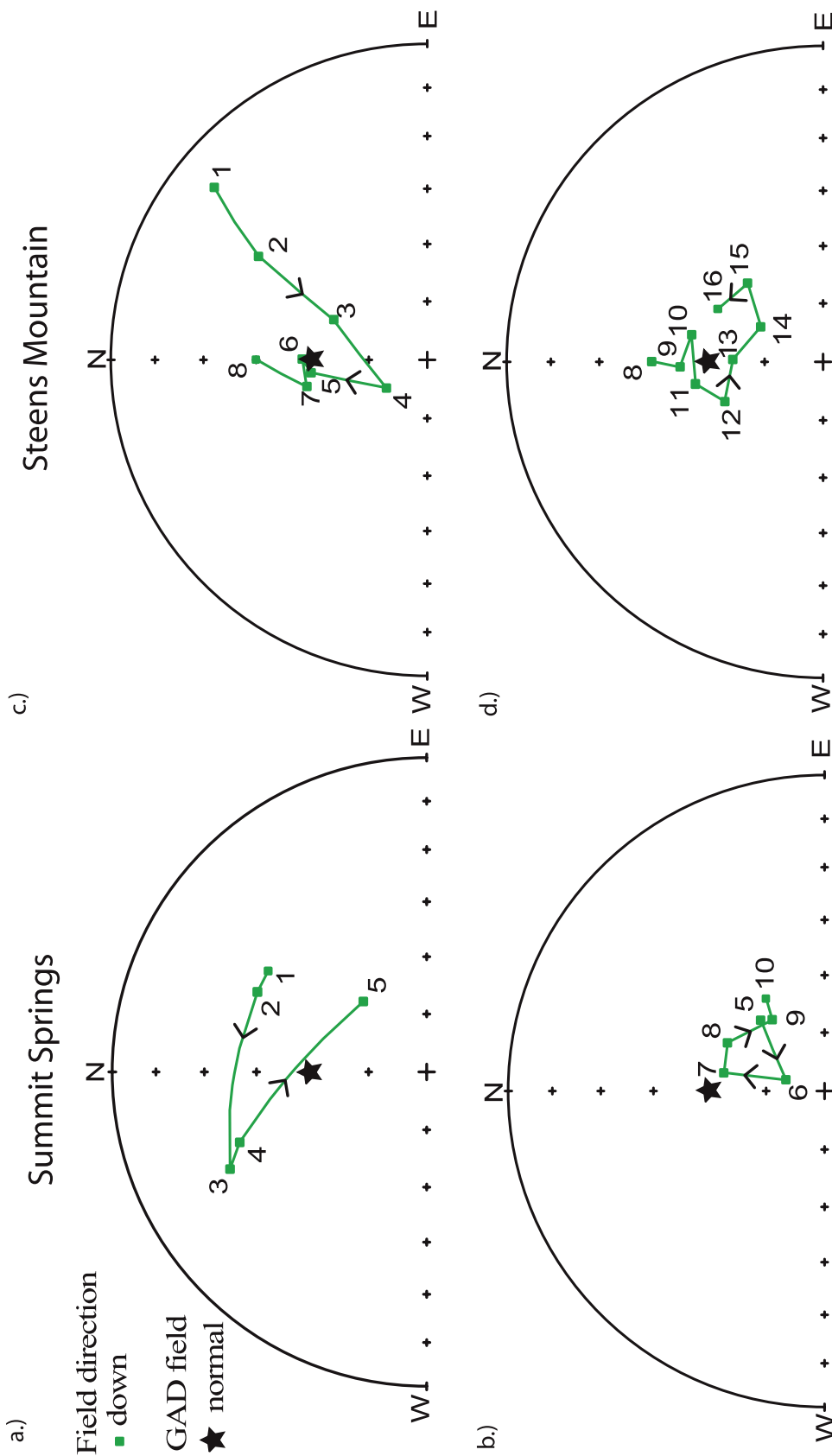


**Figure 6.** The paleomagnetic field path at Summit Springs and Steens Mountain. See text for discussion.

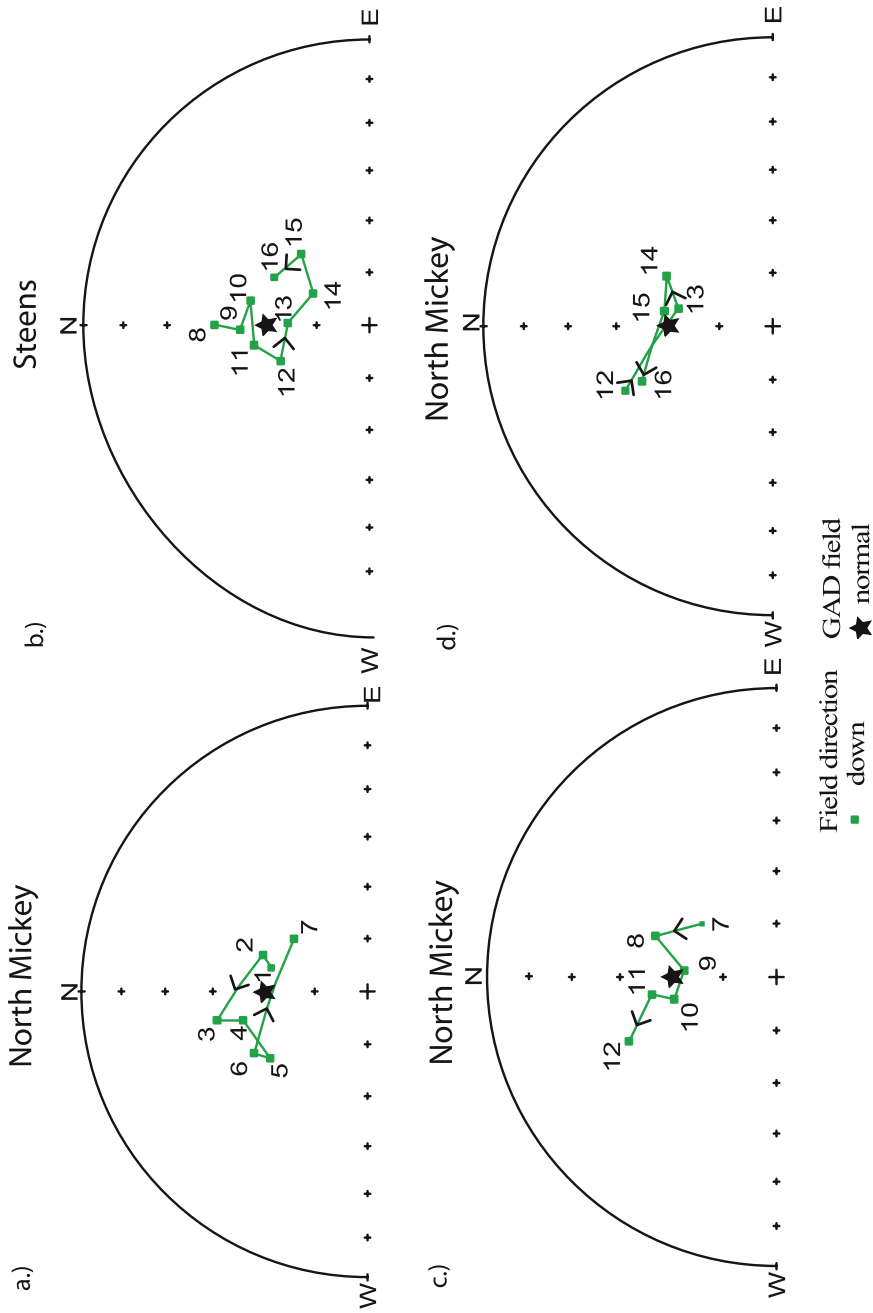


**Figure 7.** The paleomagnetic field path at North Mickey is similar to the end of the path at Steens Mountain. See text for discussion.

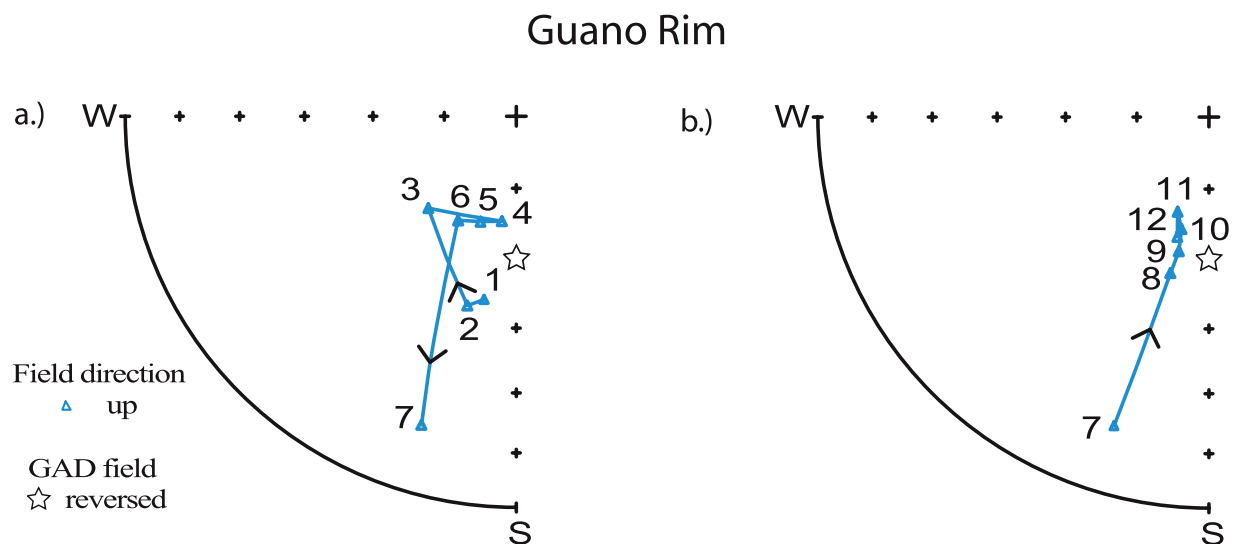


**Figure 8.** The paleomagnetic field path at Guano Rim suggests a short eruption duration. See text for discussion.

is established on the basis of a paleomagnetic reversal observed in the two areas, and supported by petrologic observations and chemical analysis” [Hook, 1981, p. 2]. He found two reverse polarity flows below seven normal polarity flows at Mickey Butte 7.5 km southwest of the North Mickey section. Two  $^{40}\text{Ar}/^{39}\text{Ar}$  dates from groundmass separates (a reverse lava  $16.69 \pm 0.18$  Ma (16.58), a normal lava  $16.59 \pm 0.30$  Ma (16.48)) by Brueseke *et al.* [2007] suggest the reversal at Mickey Butte is the Steens reversal. On inspection the Mickey Butte section has extensive cover between outcropping flows. Only a few flows are exposed in the 60 m section between the reverse polarity flow at 1470 m and the normal polarity flow at 1530 m. Looking for transitional lavas erupted during the Steens reversal, the better exposed flow-on-flow section at North Mickey was drilled. While only normal polarity lavas were found at the North Mickey location, stratigraphic continuity and the Steens-like character (large 2–4 cm plagioclase crystals) of the lower flows suggest that these lavas erupted soon after the Steens reversal.

[18] The 320 m North Mickey section consists of approximately 35 normal polarity flow-on-flow lavas in a well-exposed section. Every flow of the first 16 from the bottom was sampled for paleomagnetic analysis. Some flows at the top of the section were skipped as we believed to have already sampled through any potential reversal. The last two flows near the top were not Steens-like: aphyritic, fine grained, and weathering to a reddish brown color. The AF-demagnetization data

for all samples from this section were very well-behaved (Figure 2a). Only eight great circle fits were used from a total of 128 samples and only one sample direction was discarded. Paleomagnetic directions are given in Table 1.

[19] Once again movement of the magnetic field during the eruption of the section suggests that the flows were erupted over a short period of time. The first seven directions (DGs 1–7) make one counterclockwise loop of the magnetic field, which represents an estimated 500–1500 years based on modern analogs (Figure 7a). The youngest flows at Steens (Figure 7b) also loop in this way (DGs 10–16), suggesting that the North Mickey flows may have erupted during the same period of time as the uppermost flows found at Steens Mountain. Provided this correlation is correct, the North Mickey section preserves flows younger than the youngest flows found at Steens Mountain. From near the last directions recorded at Steens, the directions at North Mickey move to the northwest (DGs 7–12) (Figure 7c). This could imply about half the previous loop duration of about 750 years. The last four directions (DGs 13–16) record a movement back to slightly east of the GAD field direction before returning to the northwest (Figure 7d). Because this behavior appears less continuous, the eruption rate may have been much lower for this upper part of the section. The number of skipped flows and the change in petrology for the upper two flows precludes estimating the duration of eruption for this part of the section based on secular variation. In conclusion the bottom 17 flows (170 m) at the North Mickey location erup-

**Table 2.** Directional Group and VGP Means for the Four New Localities and Steens Mountain Plus Various Reference Poles<sup>a</sup>

Pole Locations	N	D°	I°	k	$\alpha_{95}$	Long°	Lat°	K	A <sub>95</sub>	S	S–	S+
Summit Springs <sup>b</sup> (ss)	11	18.6	60.0	12.6	13.4	321.9	74.0	8.6	16.5	27.6	–10.8	6.0
Pueblo Mountains (pm)	11	190.2	–59.9	31.1	8.3	146.7	–83.5	20.7	10.3	17.8	–7.0	3.9
North Mickey (nm)	16	356.9	57.6	39.1	6.0	84.3	85.6	21.3	8.2	17.6	–5.3	3.0
Guano Rim (gr)	12	197.4	–58.7	30.5	8.0	148.5	–76.8	33.0	7.7	14.1	–5.2	3.0
ss-pm-nm-gr Normal	26	4.4	58.2	20.3	6.4	0.3	84.9	12.2	8.5	23.2	–6.0	3.7
ss-pm-nm-gr Reversed	24	194.7	–60.0	30.8	5.4	142.9	–79.3	24.3	6.1	16.4	–4.0	2.7
ss-pm-nm-gr All <sup>c</sup>	50	9.2	59.2	24.1	4.2	335.1	82.5	15.9	5.2	20.3	–3.2	4.1
Steens Normal <sup>d</sup>	14	4.0	61.9	42.9	6.1	304.1	86.7	21.0	8.9	17.7	–6.0	3.6
Steens Reversed <sup>d</sup>	12	168.4	–65.2	27.1	8.5	10.4	–79.9	12.5	12.8	22.9	–8.5	4.9
Steens All <sup>c,d</sup>	26	357.3	63.6	32.6	5.0	213.8	85.8	15.4	7.5	20.7	–5.4	3.3
Oregon Plateau <sup>e</sup>	76	5.4	60.8	25.6	3.3	318.4	85.7	15.1	4.3	20.8	–2.4	2.2
High Plains <sup>d</sup>	28					209.0	88.3	19.9	6.3	18.2	–4.7	2.9
CRBG <sup>f</sup>	59					171.6	88.7	22.9	4.0	16.9	–2.5	1.9
North American Plate <sup>g</sup>	24					163.0	83.6		3.2			

<sup>a</sup>N is the number of sites in the mean, Long (Lat) is the longitude (latitude) of the VGP mean, K is the precision parameter of the mean VGP, A<sub>95</sub> is 95% confidence limit on the VGP mean, S is the angular dispersion, S–(+) is 95% negative (positive) confidence interval of the angular dispersion determined from Cox [1969].

<sup>b</sup>The antipode of the reversed polarity flow ss18 used; flow ss10 is excluded as transitional.

<sup>c</sup>The antipodes of reversed polarity flows used.

<sup>d</sup>Mankinen *et al.* [1985] DGs 1–14 (normal) and 44–55 (reversed) as determined by Prévot *et al.* [1985].

<sup>e</sup>Mean from all nontransitional groups at Steens, ss, pm, nm, and gr.

<sup>f</sup>Columbia River Basalt Group Mean from flows selected by Mankinen *et al.* [1989].

<sup>g</sup>The 15 Ma synthetic reference pole from Besse and Courtillot [2002].

ted in about 1000–3000 years and may overlap in time with the end of the Steens record. The next two flows are Steens-like and probably erupted within a few tens of thousands of years after the Steens reversal. The top two flows are not Steens-like and probably erupted within 1 Ma of the Steens reversal based on mapping by Hook [1981] and lava ages from Brueseke *et al.* [2007].

#### 6.4. Guano Rim

[20] The section at Guano Rim (42.1°N, 119.5°W) is 95 km southwest of Steens Mountain in the middle of a 20 km long escarpment. It consists of about 50 flow-on-flow reverse polarity lavas sampled 160 m up a small canyon (Figure 4). These samples were taken much earlier than the other sections, in 1986 and 1988, and their paleomagnetic directions determined at the U.S. Geological Survey (Menlo Park, California). Test samples were progressively AF-demagnetized in peak fields up to 80 mT. Each flow was magnetically cleaned at a peak alternating field chosen on the basis of behavior during the progressive demagnetization experiments (the stable endpoint method) to remove viscous and lightning strike overprints. Directions for each flow are given in Table 1. The samples are very well behaved with *k* values

for the flows varying from 103 to 1900 and only three flows with *k* < 200.

[21] Once again based on secular variation considerations these Steens-like lavas seem to have erupted over a short period of time. The first six directions (DGs 1–6) make one small loop to the west of the expected GAD field direction, suggesting 500–1500 year duration (Figure 8a). Then the field moved to a southwest and shallower direction before returning to another tight group (DGs 8–12) in a similar direction to the first (Figure 8b). This second movement suggests a duration of about 1000–2000 years, so the duration of the eruptions at Guano Rim may be ~3000 years.

### 7. Locality Means, Stability Tests, and Averaging of Secular Variation

[22] Table 2 contains mean directions and VGPs for the four localities. Both polarities are well represented, and the directions pass reversal tests. At the two northern localities the flows are all normal polarity except for one stratigraphically isolated flow (ss18, Table 1) at Summit Springs discussed earlier, whereas at the two southern localities the flows are entirely reverse. The means of the opposite polarity flows differ from antiparallel by 5.4°, well under the critical value of 8.4°

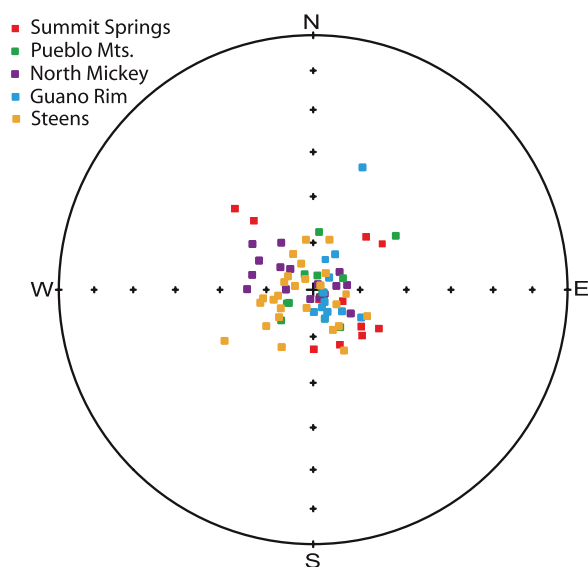


**Figure 9.** Nontransitional site mean directions for the four new localities of this study and for Steens Mountain [Mankinen *et al.*, 1985]. For reversed directions the antipodes are plotted. The directions have been rotated so that the mean of the distribution is at the center of the equal area projection.

for distinguishability at 95% confidence [McFadden and McElhinny, 1990]. Because only one fifth of the flows required tilt correction (the Pueblo Mountains section, dipping only  $20^\circ$ ), a strong fold test is precluded, but even so the improvement in clustering upon untilting ( $k_1/k_2 = 1.19$ ) is significant at 76% confidence. In light of these stability tests and the straightforward behavior of the great majority of samples during progressive demagnetization, these lava flows have almost certainly preserved reliable directions of the geomagnetic field at the times they cooled.

[23] Figure 9 shows the grouped flow directions that constitute the means in Table 2 for the four new localities and also Steens Mountain. For reverse directions the antipodes are plotted and all the directions have been rotated so that the mean of the entire distribution is at the center of the equal area projection. Although secular variation is not well averaged at any one of the four localities, due to rapid eruption rates, a compilation of all four sections should do a much better job. The total eruptive time for the continuous parts of the four sections is probably 6–10 ka, distributed on both sides of a polarity transition estimated to have taken  $4400 \pm 900$  years [Mankinen *et al.*, 1985]. In addition, directions are included from the nine flows that are not demonstrably part of the “continuously” emplaced sections, but for which age

and polarity indicate that they were erupted within a million years of the transition, most of them probably much closer. The shape of the distribution, which does not depart greatly from circular symmetry, resembles that expected for the time-averaged field at the latitude ( $43^\circ\text{N}$ ) of Steens Mountain [e.g., Tauxe and Kent, 2004, Figure 5]. This is true for our four new localities combined, for the Steens Mountain locality itself, and for all of them together (Figure 9). Moreover, the angular dispersions of VGPs for all three data sets (Table 2) agree well with the expected range of  $20.0\text{--}22.6^\circ$  from analyses of 5–22.5 Ma global lava flow data [McFadden *et al.*, 1991].

[24] These VGPs, corresponding to the directions in Figure 9, are plotted in Figure 10. Note that the transformation to VGPs maps the approximately circular distribution of directions into a distribution that is distinctly elongated. Although differing amounts of tectonic rotation about a vertical axis could also produce elongation in this same orientation, the agreement with expected shape and amount of secular variation of directions described above suggests that little or no such movement has occurred between the localities. Even stronger testimony against substantial differential tectonic rotation is the comparable elongation in VGP distribution of the pretransitional and posttransitional flows of Steens Mountain itself (Figure 10), which are from a single structural block. In conclusion, all evidence indicates that the distribution

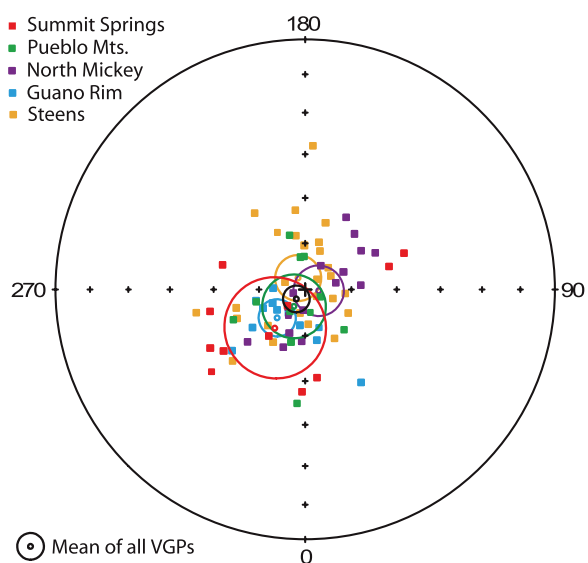


**Figure 10.** Site mean north virtual geomagnetic poles for the four new localities of this study and for Steens Mountain [Mankinen *et al.*, 1985]. Locality mean poles and corresponding circles of 95% confidence are shown.

of directions and associated VGPs provides a representative time average of middle Miocene secular variation sufficient to yield a good estimate of the geocentric axial dipole field for the region.

## 8. Mid-Miocene Pole and Rotation of the Oregon Plateau

[25] Our new data from the four localities invite a reexamination of the question whether the Oregon Plateau has rotated relative to cratonic North America. The mean paleomagnetic pole for our 50 directional groups and the 26 nontransitional directional groups at Steens Mountain defines a high-quality paleomagnetic pole (Table 2) that represents a large portion of the central Oregon Plateau (Figure 1). Omitted are several much older, smaller-scale studies that likely were not performed to the same standards. This Oregon Plateau paleomagnetic pole is  $5.1^\circ$  from the High Plains pole used by *Mankinen et al.* [1987], which consists almost entirely of VGPs from Steens Mountain and is very close to the Steens pole in Table 2. Those authors also compiled results from studies published in the 1960s and 1970s for 59 presumably unrotated flows of the Columbia River Basalt Group (CRBG pole in Table 2). These flows are on average only one million years younger than the Steens Basalt and lie farther north in Washington and northernmost Oregon. The CRBG and High Plains poles are almost identical, and so they concluded that no significant rotation ( $0.4^\circ \pm 7.6^\circ$ ) occurred between the south central Oregon Plateau and the CRBG block of southeast Washington since mid-Miocene time. Our new Oregon Plateau pole, however, implies clockwise rotation of  $7.5^\circ \pm 5.9^\circ$  relative to the CRBG.

[26] In addition, the paleomagnetic pole for the CRBG block might not be strictly representative for the North American craton. There is a paucity of other useful data of appropriate age from North America itself, but by reconstructing the relative positions of the plates using seafloor magnetic anomalies, mid-Miocene data from other continents become available. Using this method, *Besse and Courtillot* [2002] provide a 15 Ma synthetic pole for the North American plate (Table 2). Relative to it the Oregon Plateau pole is rotated  $14.5^\circ \pm 5.4^\circ$  clockwise.

[27] These new estimates for Oregon Plateau rotation reopen an early suggestion by *Magill and Cox* [1980, 1981] that south central Oregon rotated about  $10^\circ$  clockwise relative to southeast Wash-

ington since 20 Ma because of E-W extension of the basin and range that decreases to zero northward. The High Plains result of *Mankinen et al.* [1987] appeared to rule out that hypothesis. Nonetheless, several later studies revived the idea of a basin and range extension contribution to clockwise rotation of the Oregon Coast Range and pushed the boundary of the rotated block to western Oregon so as to respect the conclusion that Steens Mountain had not rotated [e.g., *Wells and Heller*, 1988]. Our new pole for the Oregon Plateau, however, indicates  $7.5^\circ$  clockwise rotation relative to the CRBG pole of southeast Washington and  $14.5^\circ$  relative to the synthetic pole for North America. It is derived from almost three times the number of directional groups, including those for Steens Mountain, and represents a much larger area of the Oregon Plateau. Northward decreasing basin and range extension still appears to be the most likely mechanism for explaining such clockwise rotation. The opening of the Oregon-Idaho graben is one well-studied example, its extension dated between 15.3 Ma and 10.5 Ma and dying out to the north in central Oregon [*Cummings et al.*, 2000].

## 9. $^{40}\text{K}$ Decay Constant and FCs Age Discussion

[28] The conventional age of the Fish Canyon sanidine (FCs) agreed upon by the Earthtime community is  $28.02 \pm 0.28$  Ma ( $1\sigma$  as per the uncertainty convention used in this paper, including the uncertainty in the decay constant [*Renne et al.*, 1998]). A more precise age for the FCs ( $28.201 \pm 0.046$  Ma, decay constant uncertainties included) has been determined by intercalibration with the astronomical timescale [*Kuiper et al.*, 2008]. The determination of this age is insensitive to the  $^{40}\text{K}$  decay constant value and any more accurate age of the FCs determined in the future is unlikely to fall outside of the above uncertainties. Other uncertainties in determining an  $^{40}\text{Ar}/^{39}\text{Ar}$  age are now likely to dominate. This FCs age is also in close agreement with an independent determination of the FCs age of  $28.28 \pm 0.06$  Ma [*Mundil et al.*, 2006] by intercalibration with the U/Pb dating system.

[29] The conventional  $^{40}\text{K}$  decay constant value of  $5.543 \times 10^{-10}/\text{a}$  (sum of  $\lambda_{\beta^-}$  and  $\lambda_{\text{E}}$ ) stated by *Steiger and Jager* [1977] is from *Beckinsale and Gale* [1969 p. 293] with a  $^{40}\text{K}$  half-life ( $T_{1/2}$ ) of  $1.265 \pm 0.0020$  for “young” ages (*Beckinsale and Gale* state “... the error in T as a result of errors in  $\lambda_{\text{E}}$  and  $\lambda_{\beta^-}$  is never greater than about  $\pm$

**Table 3.** List of Ages Found in the Paper and Alternative Ages Based on Different  $^{40}\text{K}$  Decay Constants and Fish Canyon Sanidine Ages<sup>a</sup>

Location	Sample	Earthtime Convention <sup>b</sup>		This Paper <sup>c</sup>		Alternative <sup>d</sup>		Alternative <sup>e</sup>	
		Age (Ma)	Error ( $\pm$ )	Age (Ma)	% Change	Age (Ma)	% Change	Age (Ma)	% Change
flow pma	03PMA	16.404	0.042	16.511	0.651	16.510	0.645	16.557	0.930
flow pm10	03PM10C	16.61	0.21	16.72	0.651	16.72	0.644	16.76	0.930
flow ss02	03SS02	16.61	0.28	16.72	0.651	16.72	0.644	16.76	0.930
flow ss09	03SS09G-1	17.03	0.36	17.14	0.651	17.14	0.644	17.19	0.930
flow ss09	03SS09G-2	16.60	0.38	16.71	0.651	16.71	0.644	16.75	0.930
flow ss09 <sup>f</sup>	weighted mean	16.83	0.26	16.94		16.94		16.98	
flow ss17	03SS17A-y	9.693	0.020	9.756	0.652	9.756	0.646	9.783	0.931
flow ss17	03SS17A-o	9.747	0.022	9.810	0.652	9.810	0.646	9.838	0.931
Steens reversal <sup>f</sup>	Four flows [Jarboe et al., 2006]	16.58	0.14	16.69		16.69		16.73	

<sup>a</sup>The age of the Steens reversal also included. See text for details and Table S2 for calculations. FCs is Fish Canyon Sanidine, pm is the Pueblo Mountains, and ss is Summit Springs.

<sup>b</sup>The  $^{40}\text{K}$  decay constant is from Steiger and Jager [1977]; FCs age from Renne et al. [1998].

<sup>c</sup>The  $^{40}\text{K}$  decay constant is from Min et al. [2000]; FCs age is from Kuiper et al. [2008].

<sup>d</sup>The  $^{40}\text{K}$  decay constant weighted mean is from Grau Malonda and Grau Carles [2002] and Kossert and Gunther [2004]; FCs age is from Kuiper et al. [2008].

<sup>e</sup>The  $^{40}\text{K}$  decay constant and FCs age is from Mundil et al. [2006].

<sup>f</sup>Alternative ages using 0.651%, 0.644%, and 0.930% changes to the age.

1.6% at the 95% confidence level”) adjusted for  $^{40}\text{K}$  abundance in the work of Garner et al. [1976]. Using the 1.6% uncertainty, we get a decay constant of  $5.543 \pm {}^{95} 0.089 \times 10^{-10}/\text{a}$ . This decay constant was updated to  $5.463 \pm \pm 0.107 \times 10^{-10}/\text{a}$  by Min et al. [2000] using new values for various physical constants and a statistically rigorous analysis of the underlying activity data. This  $^{40}\text{K}$  decay constant has much higher uncertainties than the reproducibility afforded by current analytical techniques and methods. Motivated in part by the geochronological community, two experiments to directly measure the  $^{40}\text{K}$  half-life by liquid scintillation counting (LSC) techniques give  $T_{1/2} = 1.248 \pm {}^{95} 0.004 \times 10^9$  a [Grau Malonda and Grau Carles, 2002] and  $T_{1/2} = 1.248 \pm {}^{95} 0.003 \times 10^9$  a [Kossert and Gunther, 2004]. Converting these half-lives to decay constants and taking the weighted mean (although the two experiments have some correlated error), we calculate a  $^{40}\text{K}$  decay constant of  $5.5541 \pm \pm 0.010 \times 10^{-10}/\text{a}$ . This value is in agreement with the geologically determined value of  $5.530 \pm \pm (7\%) \times 10^{-10}/\text{a}$  [Mundil et al., 2006].

[30] Nominal ages in this study were determined using 28.02 Ma [Renne et al., 1998] for FCs and

the Steiger and Jager [1977] decay constant. A more accurate representation of our results, we believe, is given by the astronomically calibrated age of Kuiper et al. [2008] for FCs and the Steiger and Jager updated by Min et al. [2000] value for the  $^{40}\text{K}$  decay constant. These preferred ages are most appropriate for comparison with the GTS2004 timescale, as discussed in section 11. For a summary of the ages using different  $^{40}\text{K}$  decay constants and FCs ages, see Table 3. See Figures S4 and S5 for additional plateau and isochron plots, see Table S1 for an isotopic data summary table, see Table S2 for an age adjustment calculation spreadsheet, and see Table S3 for a spreadsheet with extended isotopic data and plots.

## 10. $^{40}\text{Ar}/^{39}\text{Ar}$ Results

### 10.1. Summit Springs

[31] The second lava flow from the top of the section (ss02, Figure 4) has a normal polarity and an  $^{40}\text{Ar}/^{39}\text{Ar}$  plateau age of  $16.72 \pm \pm 0.28$  Ma (16.61) from a plagioclase separate (Figure 11a). The 15-step plateau encompasses all of the degassing steps and is well-behaved. Inverse isochron analyses of Summit Springs lavas give ages that

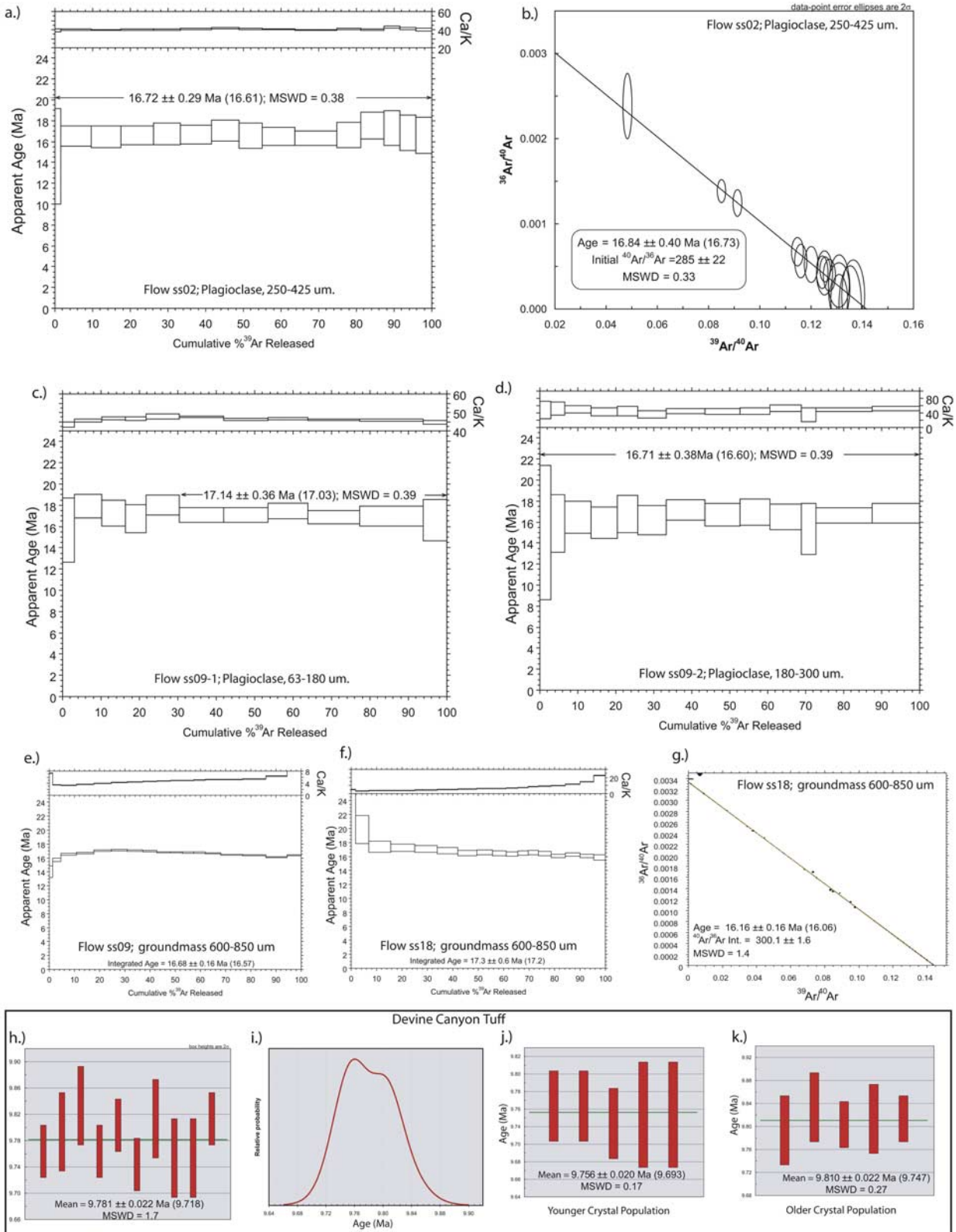
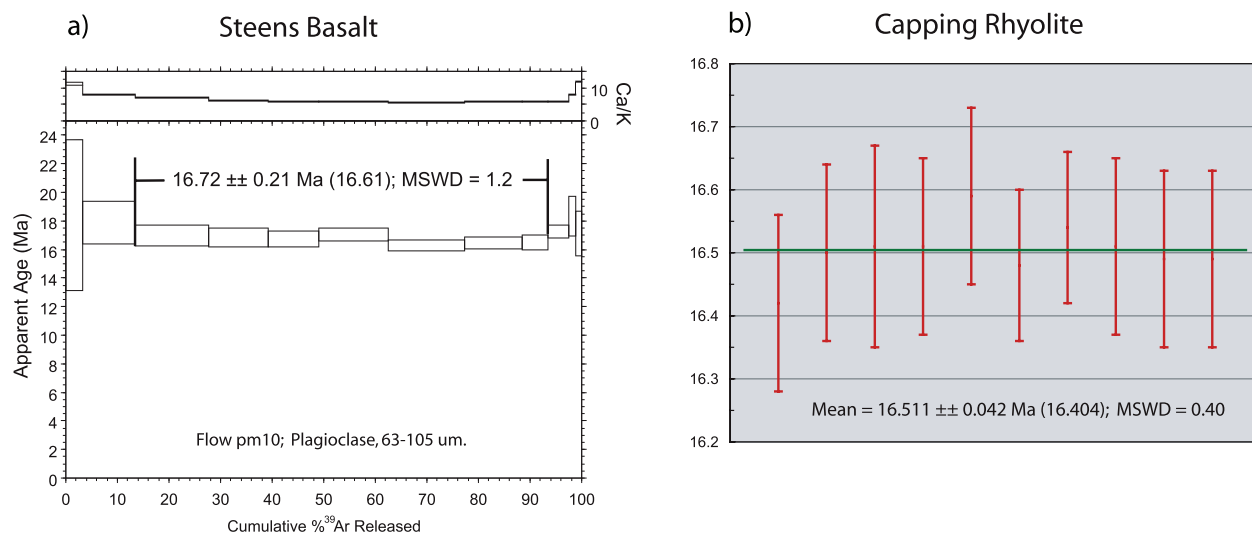


Figure 11.  $^{40}\text{Ar}/^{39}\text{Ar}$  ages from Summit Springs.



**Figure 12.**  $^{40}\text{Ar}/^{39}\text{Ar}$  ages from Pueblo Mountains.

generally agree with the plateau ages and have atmospheric  $^{36}\text{Ar}/^{40}\text{Ar}$  ratios (Figure 11b). Our determination of the age of the lava from flow ss09 was less straightforward. Plagioclase separates of two different size fractions from the same sample were dated (Figures 11c and 11d). The smaller size fraction (63–180  $\mu\text{m}$ ) was analyzed first because smaller grains generally have higher potassium and lower calcium concentrations and therefore lower age uncertainties. A single degassing analysis gave two plateau ages with the criteria described in section 5. A younger plateau consisting of the last six degassing steps gave an age of  $17.14 \pm 0.36$  Ma (17.03) while an older plateau consisting of the first eight degassing steps gives an age of  $17.39 \pm 0.38$  Ma (17.28). The younger age plateau has more radiogenic gas released, smaller uncertainties, and higher probability so we choose it as the age of this degassing analysis. The age was older than expected, given its normal polarity and Steens-like appearance, so the larger-size fraction (180–300  $\mu\text{m}$ ) was analyzed (Figure 11d). This analysis again gave a good plateau age ( $16.71 \pm 0.38$  Ma (16.60)). The larger uncertainty in the Ca/K ratio is due mostly to the larger uncertainties in the  $^{37}\text{Ar}$  (half-life 35.0 days) abundances because this analysis was performed 9 months after the smaller size fraction. This age is 0.43 Ma younger than the previous age but their  $2\sigma$  errors overlap by 0.31 Ma. While we suspect that the plateau age of the larger size fraction is more likely correct, the weighted mean of the two ages ( $16.92 \pm 0.26$  Ma (16.83)) is the most objective  $^{40}\text{Ar}/^{39}\text{Ar}$  age for flow ss09 although using a weighted mean may underestimate the uncertainty.

[32] Given the issues described above we also analyzed some groundmass separates from this flow. The generally lower Ca/K of groundmass separates allows for greater precision on each heating step, but often alteration and/or recoil effects can prevent good plateaus from being produced. Two groundmass step-heating analyses yielded disturbed spectra likely due to recoil effects. In both cases (one spectrum shown in Figure 11e) the step ages start low and increase to a maximum at about 1/3 of the  $^{39}\text{Ar}$  released and then slowly decrease in age. When only groundmass samples are available and the age spectra are disturbed, the total gas integrated age may define a valid eruption age, provided that alteration is insignificant and recoil effects are limited to argon isotope redistribution within, rather than net loss from, the sample. Our integrated ages for two groundmass analyses are  $16.63 \pm 0.16$  (16.52) Ma and  $16.68 \pm 0.16$  Ma (16.57). These ages are consistent with the weighted mean of the two plagioclase separate ages but, given our inability to verify the abovementioned criteria for validity, we do not include the ages in the weighted mean age of the lava.

[33] Two other eruptive units from the Summit Springs section were also dated. The first is the Devine Canyon Tuff (V. Camp, personal communication, 2005), which covers the flat area at the bottom of the section (ss17, Figure 4). Ages of 10 single-crystal sanidine grains were determined by step-heating (Figure 11h) and have a weighted mean age of  $9.781 \pm 0.022$  Ma (9.718) that is much younger than the Steens lavas. These very

precise ages fall into two groups (Figures 5i, 5j, and 5k) with ages of  $9.756 \pm 0.020$  Ma (9.693) and  $9.810 \pm 0.022$  Ma (9.747), suggesting an eruption age for the Devine Canyon Tuff of  $9.756 \pm 0.020$  Ma (9.693) and xenocrystic contamination of the tuff with a population of crystals only 54 ka older. The second is from a basaltic lava of reverse polarity about 1 km east of the main section (ss18, Figure 4). Age determinations from a plagioclase separate were inconclusive (not shown), and a groundmass age spectrum is disturbed with an integrated age of  $17.3 \pm 0.6$  Ma (17.2) (Figure 11f). Its isochron age is better defined at  $16.16 \pm 0.16$  Ma (16.06) (Figure 11g). Summarizing the most pertinent points of the Summit Spring ages, the two lavas dated in the upper section erupted near the 16.6 Ma Steens reversal while the more isolated reverse polarity lava erupted within 1 Ma of the Steens reversal.

## 10.2. Pueblo Mountains

[34] An  $^{40}\text{Ar}/^{39}\text{Ar}$  age of  $16.72 \pm 0.21$  Ma (16.61) was determined from a plagioclase separate of the reverse polarity flow pm10 (Figure 12a). As found at Summit Springs, this age is indistinguishable from that of the 16.6 Ma Steens reversal. The dated sample lies stratigraphically below the continuous section. The age of the section is also constrained by a  $16.511 \pm 0.042$  Ma (16.404) age from the weighted mean of 10 step-heated sanidine grains from a reverse polarity rhyolite located at the top of the section (Figure 12b).

## 11. Comparing Ages to the Geomagnetic Polarity Timescale

[35] The boundaries for geomagnetic polarity chrons for much of the Neogene have been determined from the astronomical tuning of deep-sea ocean cores that have magnetic signatures. These studies have been compiled into a composite geomagnetic polarity timescale (GPTS) in the work of *Gradstein et al.* [2004]. For Neogene times before the C5Ar.3r chron (12.878 Ma) the chron boundaries of *Gradstein et al.* [2004] were determined using a seafloor-spreading-rate history model of the Australia-Antarctic plate pair with astronomically tuned tie points at the top of C5Ar.3r from *Abdul-Aziz et al.* [2003], the top and bottom of C5Br from *Shackleton et al.* [2001], and a recalculated 23.03 Ma Oligocene-Miocene boundary from *Shackleton et al.* [2000] using the La2003 orbital model. A potentially better GPTS for the early and mid-Miocene is was determined by *Billups et al.*

[2004] from orbitally tuned Ocean Drilling Program (ODP) Site 1090 cores that have a magnetic signature. Their study should give more accurate astronomical time boundaries to early Neogene chrons, but the chrons relevant for this study are at the very top of the cores and have low sedimentation rates. Both of these factors tend to make the chron boundaries less reliable and we choose to compare to the *Gradstein et al.* [2004] GPTS (Figure 13), which generally agrees with *Billups et al.* [2004] to one precession cycle ( $\sim 20$  ka).

[36] The younger normal polarity lava at Summit Springs (ss02) likely erupted in the C5Cn.3n chron after the Steens reversal. Its errors (at two sigma confidence) encompass all of the C5Cn.3n normal chron, reach 1/3 into the younger C5Cn.2n normal chron, and do not reach the older C5Dn normal chron (Figure 13). The two sigma errors of the weighted mean  $^{40}\text{Ar}/^{39}\text{Ar}$  age for the normal polarity lava ss09 encompass most of the reversed C5Cr chron and one third of the of the normal C5Cn.3n chron. Barring any unknown normal cryptochron during the reverse C5Cr chron and considering the younger groundmass integrated ages, the lava is most likely to have erupted in the C5Cn.3n chron after the Steens reversal. This interpretation is also supported by the similarities between the Summit Springs magnetic field path and Steens Mountain postreversal magnetic field path. At Pueblo Mountains the reverse polarity flow pm10 likely erupted during the C5Cr chron before the Steens reversal, although the two sigma errors of the  $^{40}\text{Ar}/^{39}\text{Ar}$  age reach into the short C5Cn.2r after the Steens reversal. The younger and more precise age of the reverse polarity capping rhyolite (pma) at Pueblo Mountains unequivocally places its eruption during the C5Cn.2r chron, indicating that no eruptions took place at this section during the 170 ka-long C5Cn.3n [*Gradstein et al.*, 2004] normal polarity chron.

## 12. Conclusions

[37] Paleomagnetic analyses and  $^{40}\text{Ar}/^{39}\text{Ar}$  ages from Pueblo Mountains, Summit Springs, North Mickey, and Guano Rim suggest that the bulk of these sections were erupted in short bursts ( $\sim 1-3$  ka) within  $\sim 300$  ka of the Steens reversal. Comparison to the geomagnetic polarity timescale (Figure 7) and two  $^{40}\text{Ar}/^{39}\text{Ar}$  ages (Table 3) show that the Pueblo Mountains reverse section erupted near and likely before the Steens reversal. Comparing the simple directional path of the remanent magnetization with secular variation of the recent

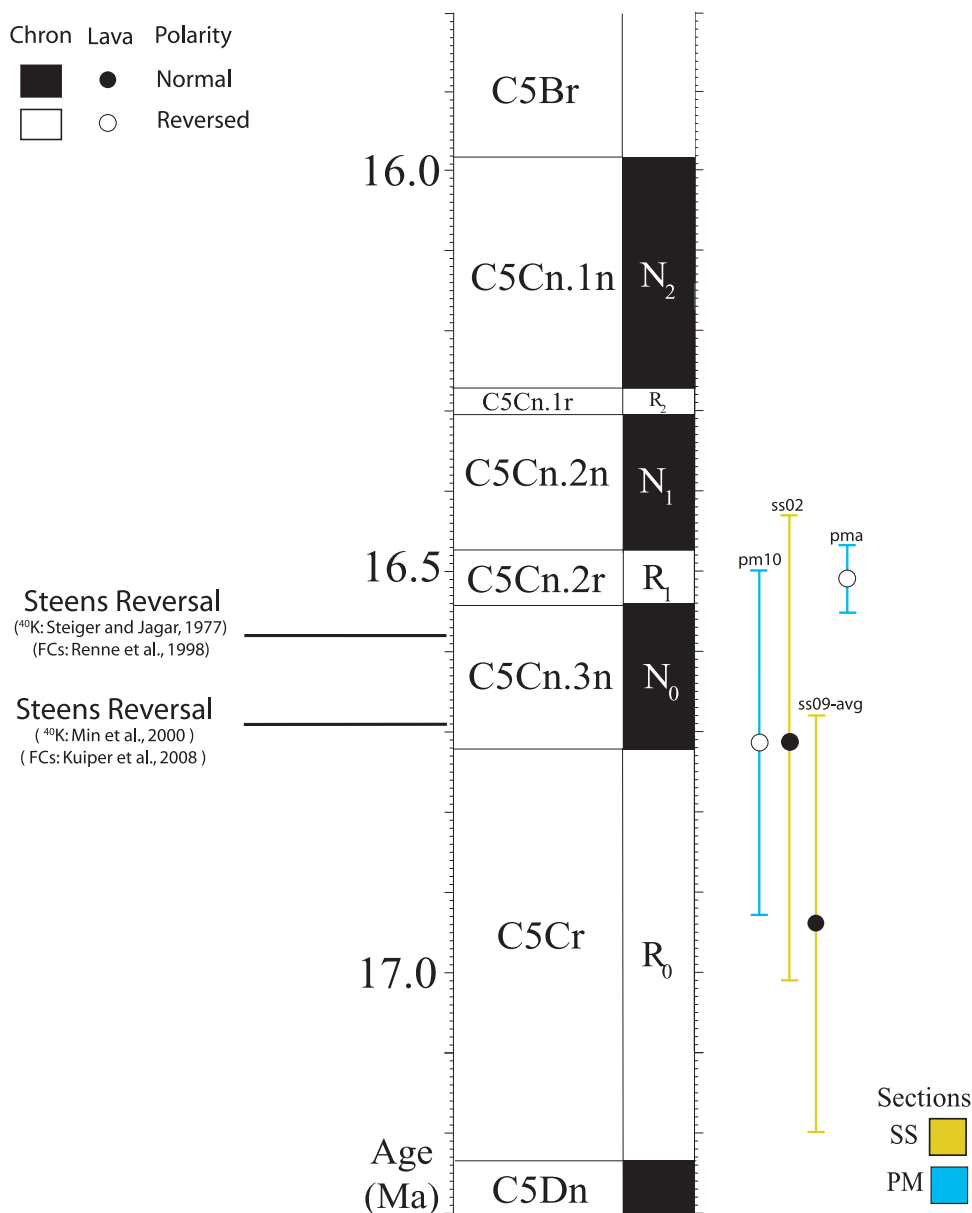


**Figure 13.**  $^{40}\text{Ar}/^{39}\text{Ar}$  ages from the text have been displayed with their uncertainties for comparison to the geomagnetic polarity timescale of *Gradstein et al.* [2004]. Both the ss02 and ss09 flows at Summit Springs are most likely to have erupted after the Steens reversal during the C5Cn.3n chron. At Pueblo Mountains the basalts (pm10) are likely to have erupted before the Steens reversal during the C5Cr chron while the capping rhyolite at Pueblo Mountains (pma) erupted during the next reverse chron (C5Cn.2r). Columbia River Basalt magnetostratigraphy is shown with the Steens Reversal placed at the top of the C5Cr chron. See text for further discussion. SS, Summit Springs, PM, Pueblo Mountains.

field indicates that the continuously sampled section erupted in about 2.5 ka. At Summit Springs two  $^{40}\text{Ar}/^{39}\text{Ar}$  ages, dominantly normal polarity (all but one stratigraphically isolated flow), and the simple directional path suggest that the section erupted in the chron after the Steens reversal within about 0.5 to 1.5 ka. At North Mickey geologic mapping and dates by others place the section near

the Steens reversal, and secular variation analysis indicates that the lower part erupted in 1–3 ka. At Guano Rim the low ( $14.1^\circ$ ) dispersion of VGPs and the directional path suggest a  $\sim 3$  ka eruption duration. The rapid eruption of these sizable sections near the time of the Steens reversal suggests that the Steens Basalts were all emplaced within a

few hundred thousand years on the Oregon Plateau at around 16.7 Ma.

[38] Although the flows at each individual locality do not average out secular variation, by combining all of the sections enough time is sampled to obtain a meaningful average paleomagnetic pole. From our four sections there are a total 26 normal and 24 reverse directions (Table 2) that yield a positive reversal test. Combining our VGP directions with the nontransitional VGPs at Steens Mountain yields a new pole for the Oregon Plateau that indicates clockwise rotation of  $7.4^\circ \pm 5.9^\circ$  with respect to the CRBG and  $14.4^\circ \pm 5.4^\circ$  with respect to cratonic North America. This implies some extension to the east of the study area since 16.7 Ma that dies out rapidly to the north.

## Acknowledgments

[39] We would like to extend special thanks to Kim Knight for assistance with  $^{40}\text{Ar}/^{39}\text{Ar}$  sample preparation and analysis methods and Chris Pluhar for assistance with paleomagnetic procedures and methods. Laurie Brown, Andy Calvert, Jim Gill, Johnathan Hagstrum, Peter Hooper, and Brad Singer provided helpful reviews which improved the clarity of this paper. We thank Eli Morris and Walter Schillinger for UCSC paleomagnetic instrumentation and software support, Tim Becker for BGC lab support, and Fred Jourdan for assistance with determining plagioclase alteration. For highly competent field work assistance we would like to thank Mike Dueck, Bijan Hatami, Peter Lippert, and Andy Daniels. This work was funded by NSF grant EAR-0310316 and -0711418 to RSC and JMG, minigrants from the UCSC Committee on Research and Institute of Geophysics and Planetary Physics, and support to the BGC from the Ann and Gordon Getty Foundation.

## References

- Abdul-Aziz, H., F. J. Hilgen, W. Krijgsman, and J. P. Calvo (2003), An astronomical polarity timescale for the late middle Miocene based on cyclic continental sequences, *J. Geophys. Res.*, *108*(B3), 2159, doi:10.1029/2002JB001818.
- Beckinsale, R. D., and N. H. Gale (1969), A reappraisal of the decay constants and branching ratio of  $^{40}\text{K}$ , *Earth Planet. Sci. Lett.*, *6*, 289–294, doi:10.1016/0012-821X(69)90170-8.
- Besse, J., and V. Courtillot (2002), Apparent and true polar wander and the geometry of the geomagnetic field over the last 200 Myr, *J. Geophys. Res.*, *107*(B11), 2300, doi:10.1029/2000JB000050.
- Billups, K., H. Palike, J. E. T. Channell, J. C. Zachos, and N. J. Shackleton (2004), Astronomic calibration of the late Oligocene through early Miocene geomagnetic polarity time scale, *Earth Planet. Sci. Lett.*, *224*, 33–44, doi:10.1016/j.epsl.2004.05.004.
- Brueseke, M. E., M. T. Heizler, and S. A. Mertzman (2007), Distribution and geochronology of Oregon Plateau (U.S.A.) flood basalt volcanism: The Steens Basalt revisited, *J. Volcanol. Geotherm. Res.*, *161*, 187–214, doi:10.1016/j.jvolgeores.2006.12.004.
- Camp, V. E., and M. E. Ross (2004), Mantle dynamics and genesis of mafic magmatism in the intermontane Pacific Northwest, *J. Geophys. Res.*, *109*, B08204, doi:10.1029/2003JB002838.
- Camp, V. E., M. E. Ross, and W. E. Hanson (2003), Genesis of flood basalts and basin and range volcanic rocks from Steens Mountain to the Malheur River Gorge, Oregon, *Geol. Soc. Am. Bull.*, *115*(1), 105–128, doi:10.1130/0016-7606(2003)115<0105:GOFBAB>2.0.CO;2.
- Carlson, R. W., and W. K. Hart (1987), Crustal genesis on the Oregon Plateau, *J. Geophys. Res.*, *92*, 6191–6206, doi:10.1029/JB092iB07p06191.
- Cox, A. (1969), Confidence limits for the precision parameter  $K$ , *Geophys. J. R. Astron. Soc.*, *18*, 545–549.
- Cummings, M. L., J. G. Evans, M. L. Ferns, and K. R. Lees (2000), Stratigraphic and structural evolution of the middle Miocene synvolcanic Oregon-Idaho graben, *Geol. Soc. Am. Bull.*, *112*(5), 668–682, doi:10.1130/0016-7606(2000)112<0668:SASEOT>2.3.CO;2.
- Deino, A. L. (2001), Users manual for Mass Spec v. 5.02, Berkeley Geochronology Cent., Berkeley, Calif.
- Enkin, R. (2005), *PMGSC 4.2*, Geol. Surv. of Canada, Sidney, British Columbia, Canada.
- Fisher, R. A. (1953), Dispersion on a sphere, *Proc. R. Soc. London, Ser. A*, *217*, 295–305.
- Fuller, R. E. (1931), *The Geomorphology and Volcanic Sequence of Steens Mountain in Southeastern Oregon*, 130 pp., Univ. of Wash. Press, Seattle, Wash.
- Garner, E. L., T. J. Murphy, J. W. Gramlich, P. J. Paulson, and I. L. Barnes (1976), Absolute isotopic abundance ratios and the atomic weight of a reference sample of potassium, *J. Res. U.S. Natl. Bur. of Stand.*, *79A*, 713–725.
- Gradstein, F., J. Ogg, and A. Smith (2004), *A Geologic Time Scale 2004*, 589 pp., Cambridge Univ. Press, Cambridge, U.K.
- Grau Malonda, A., and A. Grau Carles (2002), Half-life determination of  $^{40}\text{K}$  by LSC, *Appl. Radiat. Isot.*, *56*, 153–156, doi:10.1016/S0969-8043(01)00181-6.
- Hagstrum, J. T., and D. E. Champion (2002), A Holocene paleosecular variation record from 14C-dated volcanic rocks in western North America, *J. Geophys. Res.*, *107*(B1), 2025, doi:10.1029/2001JB000524.
- Hart, W. K., R. W. Carlson, and S. A. Mosher (1989), Petrogenesis of the Pueblo Mountains basalt, southeastern Oregon and northern Nevada, *Geol. Soc. Am. Spec. Pap.*, *239*, 367–378.
- Hook, R. (1981), The volcanic stratigraphy of the Mickey Hot Springs area, Harney County, Oregon., Master's thesis, Oregon State Univ., Corvallis.
- Hooper, P. R., G. B. Binger, and K. R. Lees (2002), Ages of the Steens and Columbia River flood basalts and their relationship to extension-related calc-alkalic volcanism in eastern Oregon, *Geol. Soc. Am. Bull.*, *114*(1), 43–50, doi:10.1130/0016-7606(2002)114<0043:AOTSAC>2.0.CO;2.
- Jarboe, N. A., R. S. Coe, P. R. Renne, and J. M. Glen (2006),  $^{40}\text{Ar}/^{39}\text{Ar}$  Ages of the Early Columbia River Basalt Group: Determining the Steens Mountain Geomagnetic Polarity Reversal (R0–N0) as the top of the C5Cr Chron and the Imnaha Normal (N0) as the C5Cn.3n Chron, *Eos Trans. American Geophysical Union*, *87*(52), Fall Meet. Suppl., Abstract V51D–1702.
- Kirschvink, J. L. (1980), The least-squares line and plane and the analysis of paleomagnetic data, *Geophys. J. R. Astron. Soc.*, *62*, 699–718.

- Kossert, K., and E. Gunther (2004), Liquid scintillation counting LSC measurements of the half-life of  $^{40}\text{K}$ , *Appl. Radiat. Isot.*, *60*, 459–464, doi:10.1016/j.apradiso.2003.11.059.
- Kuiper, K. F., A. Deino, F. J. Hilgen, W. Krijgsman, P. R. Renne, and J. R. Wijbrans (2008), Synchronizing rock clocks of Earth history, *Science*, *320*, 500–504, doi:10.1126/science.1154339.
- Ludwig, K. R. (2003), Isoplot 3.13: A geochronological toolkit for Microsoft Excel, *Spec. Publ. 4*, Berkeley Geochronology Cent., Berkeley, Calif.
- Magill, J., and A. Cox (1980), Tectonic rotation of the Oregon western Cascades, *Spec. Pap.*, *10*, 67 pp., Oreg. Dept. of Geol. and Mineral Ind., Portland, Oreg.
- Magill, J., and A. Cox (1981), Post-Oligocene tectonic rotation of the Oregon Western Cascade Range and the Klamath Mountains, *Geology*, *9*, 127–131, doi:10.1130/0091-7613(1981)9<127:PTROTO>2.0.CO;2.
- Mankinen, E. A., M. Prévot, C. S. Grommé, and R. S. Coe (1985), The Steens Mountain (Oregon) geomagnetic polarity transition: 1. Directional history, duration of episodes, and rock magnetism, *J. Geophys. Res.*, *90*(B12), 10,393–10,416.
- Mankinen, E. A., E. L. Larson, C. S. Grommé, M. Prévot, and R. S. Coe (1987), The Steens Mountain (Oregon) geomagnetic polarity transition: 3. Its regional significance, *J. Geophys. Res.*, *92*(B8), 8057–8076, doi:10.1029/JB092iB08p08057.
- Mankinen, E. A., W. P. Irwin, and C. S. Grommé (1989), Paleomagnetic study of the Eastern Klamath Terrane, California, and implications for the tectonic history of the Klamath Mountains Province, *J. Geophys. Res.*, *94*(B8), 10,444–10,472, doi:10.1029/JB094iB08p10444.
- McFadden, P. L., and M. W. McElhinny (1988), The combined analysis of remagnetization circles and direct observations in paleomagnetism, *Earth Planet. Sci. Lett.*, *87*, 161–172, doi:10.1016/0012-821X(88)90072-6.
- McFadden, P. L., and M. W. McElhinny (1990), Classification of the reversal test in paleomagnetism, *Geophys. J. Int.*, *103*, 725–729, doi:10.1111/j.1365-246X.1990.tb05683.x.
- McFadden, P. L., and M. W. McElhinny (1995), Combining groups of paleomagnetic directions or poles, *Geophys. Res. Lett.*, *22*(16), 2191–2194, doi:10.1029/95GL01441.
- McFadden, P. L., R. T. Merrill, M. W. McElhinny, and S. Lee (1991), Reversals of the Earth's magnetic field and temporal variations of the dynamo families, *J. Geophys. Res.*, *96*, 3923–3933, doi:10.1029/90JB02275.
- Min, K., R. Mundil, P. R. Renne, and K. R. Ludwig (2000), A test for systematic errors in  $^{40}\text{Ar}/^{39}\text{Ar}$  geochronology through comparison with U-Pb analysis of a 1.1 Ga rhyolite, *Geochim. Cosmochim. Acta*, *64*(1), 73–98, doi:10.1016/S0016-7037(99)00204-5.
- Mundil, R., P. R. Renne, K. K. Min, and K. R. Ludwig (2006), Resolvable miscalibration of the  $^{40}\text{Ar}/^{39}\text{Ar}$  geochronometer, *Eos Trans. AGU*, *87*(52), Fall Meet. Suppl., Abstract V21A–0543.
- Ohno, M., and Y. Hamano (1992), Geomagnetic poles over the past 10000 years, *Geophys. Res. Lett.*, *19*, 1715–1718, doi:10.1029/92GL01576.
- Prévot, M., E. A. Mankinen, R. S. Coe, and C. S. Grommé (1985), The Steens Mountain (Oregon) geomagnetic polarity transition: 2. Field intensity variations and discussion of reversal models, *J. Geophys. Res.*, *90*(B12), 10,417–10,488, doi:10.1029/JB090iB12p10417.
- Renne, P. R., C. C. Swisher, A. L. Deino, D. Karner, B. T. L. Owens, and D. J. DePaolo (1998), Intercalibration of standards, absolute ages and uncertainties in  $^{40}\text{Ar}/^{39}\text{Ar}$  dating, *Chem. Geol.*, *145*, 117–152, doi:10.1016/S0009-2541(97)00159-9.
- Rowe, W. A. (1971), *Geology of the South-central Pueblo Mountains, Oregon-Nevada*, Oreg. State Univ., Corvallis.
- Schnepp, E., and P. Lanos (2005), Archaeomagnetic secular variation in Germany during the past 2500 years, *Geophys. J. Int.*, *163*, 479–490, doi:10.1111/j.1365-246X.2005.02734.x.
- Shackleton, N. J., M. A. Hall, I. Raffi, L. Tauxe, and J. Zachos (2000), Astronomical calibration age for the Oligocene-Miocene boundary, *Geology*, *28*(5), 447–450, doi:10.1130/0091-7613(2000)28<447:ACAFTO>2.0.CO;2.
- Shackleton, N. J., I. Raffi, and U. Rohl (2001), Astronomical age calibration in the Middle Miocene, *Eos Trans. AGU*, *82*(20), Spring Meet. Suppl., Abstract OS32A-03.
- Steiger, R. H., and E. Jager (1977), Subcommittee on geochronology: Convention on the use of decay constants in geo- and cosmochronology, *Earth Planet. Sci. Lett.*, *36*, 359–362, doi:10.1016/0012-821X(77)90060-7.
- Tauxe, L., and D. V. Kent (2004), A simplified statistical model for the geomagnetic field and the detection of shallow bias in paleomagnetic inclinations: Was the ancient magnetic field dipolar?, in *Timescales of the Paleomagnetic Field*, *Geophys. Monogr. Ser.*, vol. 145, edited by J. E. T. Channell et al., pp. 101–115, AGU, Washington, D. C.
- Watkins, N. D. (1963), Behaviour of the geomagnetic field during the Miocene period in south-eastern Oregon, *Nature*, *197*(4863), 126–128, doi:10.1038/197126a0.
- Wells, R. E., and P. L. Heller (1988), The relative contribution of accretion, shear, and extension to Cenozoic tectonic rotation in the Pacific Northwest, *Geol. Soc. Am. Bull.*, *100*, 325–338, doi:10.1130/0016-7606(1988)100<0325:TRCOAS>2.3.CO;2.